Quantum Electronics **37** (5) 409 – 432 (2007)

REVIEW

PACS numbers: 42.70.Qs; 42.25.Fx; 78.35.+c
DOI: 10.1070/QE2007v037n05ABEH013478

Optics of globular photonic crystals

V.S. Gorelik

Contents

***Abstract*. The results of experimental and theoretical studies of the optical properties of globular photonic crystals – new physical objects having a crystal structure with the lattice period exceeding considerably the atomic size, are presented. As globular photonic crystals, artificial opal matrices consisting of close-packed silica globules of diameter ~ 200 nm were used. The reflection spectra of these objects characterising the parameters of photonic bands existing in these crystals in the visible spectral region are presented. The idealised models of the energy band structure of photonic crystals investigated in the review give analytic dispersion dependences for the group velocity and the effective photon mass in a globular photonic crystal. The characteristics of secondary emission excited in globular photonic crystals by monochromatic and broadband radiation are presented. The results of investigations of single-photon-excited delayed scattering of light observed in globular photonic crystals exposed to cw UV radiation and radiation from a repetitively pulsed copper vapour laser are presented. The possibilities of using globular photonic crystals as active media for lasing in different spectral regions are considered. It is proposed to use globular photonic crystals as sensitive sensors in optoelectronic devices for molecular analysis of organic and inorganic materials by the modern methods of laser spectroscopy. The results of experimental studies of spontaneous and stimulated globular scattering of light are discussed. The conditions for observing resonance and two-photon-excited delayed scattering of light are found. The possibility of accumulation and localisation of the laser radiation energy inside a globular photonic crystal is reported.**

V.S. Gorelik P.N. Lebedev Physics Institute, Russian Academy of Sciences, Leninsky prosp. 53, 119991 Moscow, Russia;
e-mail: gorelik@sci.lebedev.ru

Received 15 November 2006
Kvantovaya Elektronika **37** (5) 409 – 432 (2007)
Translated by M.N. Sapozhnikov

Keywords: *globule, light scattering, photonic crystal, forbidden band, reflection spectrum.*

1. Introduction

Ordered structures with a period a_0 comparable to the wavelength of electromagnetic radiation have long been used in optics. The examples of such structures are diffraction gratings, interference filters and multilayer dielectric mirrors. As is known from solid-state physics,

the periodicity of the structure of a material medium gives rise to the so-called energy bands in the spectrum. The optical properties of a semiconductor crystal are related to the energy gap E_g, which is equal to the difference between the energies of the valence-band top and the conduction-band bottom. The lattice period $a_0 \sim 10^{-8}$ cm in a crystalline solid is comparable with the de Broglie wavelength of an electron, and the spectrum of allowed and forbidden bands is determined by the values of possible energy states of electrons and holes.

The presence of a periodic structure in a material with a period close to the wavelength of the electromagnetic wave leads to the formation of the corresponding allowed and forbidden photonic bands. The possibility of formation of such bands was first established by Bykov [1]. Then, the features of photonic bands were analysed in papers of Yablonovich [2] and John [3]. The term 'photonic crystals' was introduced in paper [2] and is related to periodic structures in which photonic bands are formed. In fact, the above-mentioned optical structures (diffraction gratings, interference filters, multilayer dielectric mirrors) also belong to photonic crystals.

In 1991 the authors of paper [4] fabricated for the first time a three-dimensional photonic crystal by having drilled millimetre holes in a material with a high refractive index. This artificial crystal, called yablonovit, had the forbidden photonic band in the millimetre spectral region.

Photonic crystals were used for the development of new optical devices such as high-Q resonators, spectral filters, selective mirrors, nonlinear optical elements [5], etc. Of special interest are three-dimensional photonic crystals constructed from globules of the same diameter [6]. Such structures are called globular photonic crystals. A typical example of a globular photonic crystal is artificial opal consisting of amorphous silica globules forming a face-centred cubic (FCC) lattice. This review presents the results of recent experimental and theoretical studies [7–22] of the optical and nonlinear-optical properties of globular photonic crystals performed with the participation of the author.

2. Structure of globular photonic crystals

As mentioned above, a globular photonic crystal is constructed of globules of the same diameter d packed in the form of a crystal lattice (Fig. 1). Materials close in the structure to globular photonic crystals exist in nature. In particular, these are the so-called spherical viruses with the structure representing a cubic crystal lattice with the period up to 200 nm.

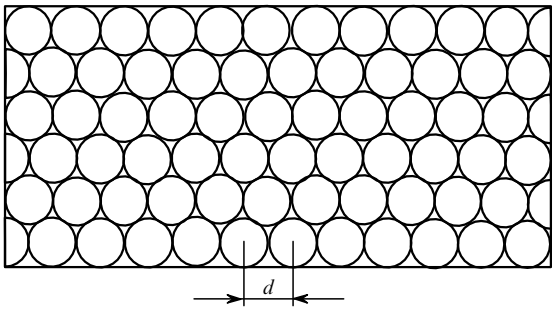

Figure 1. Schematic structure of a globular photonic crystal consisting of spherical particles (globules) closely packed into a cubic crystal lattice (d is the globule diameter).

Another example of a globular photonic crystal encountered in nature is the known mineral opal. Natural opal has a FCC lattice formed by silica globules of diameter 200–600 nm. They are regularly packed into a three-dimensional superlattice, and the system as a whole forms a three-dimensional photonic crystal. Such lattices contain structural voids (of the tetrahedral and octahedral types) of size 60–200 nm, which are filled with water and other components in natural opals.

In the 1990s the methods for synthesis of opals were developed [23–26]. The diameter of silica globules in synthetic opals can vary between 100 and 1000 nm. Bulk samples, which are quite durable and thermally stable, were synthesised by L.A. Samoilovich (Almaztekhnokristal Joint-Stock Company, Aleksandrov). These works were continued at Opalon Joint-Stock Company and TsNITI Joint-Stock Company (Moscow). Samples of artificial opal matrices for our studies were kindly placed at our disposal by M.I. Samoilovich (TsNITI JSC) and S.N. Ivicheva (Institute of Inorganic Chemistry, RAS, Moscow). The general view of synthetic opals investigated in our works is presented in Fig. 2. The electron-microscope photograph of the nanostructure of artificial opal is shown in Fig. 3.

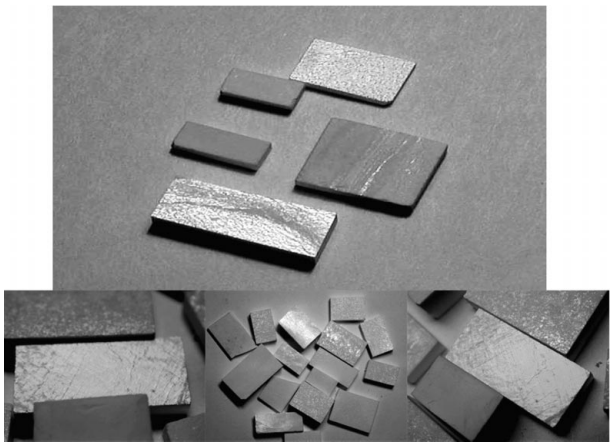

Figure 2. Photograph of artificial opals illuminated by white light at different angles.

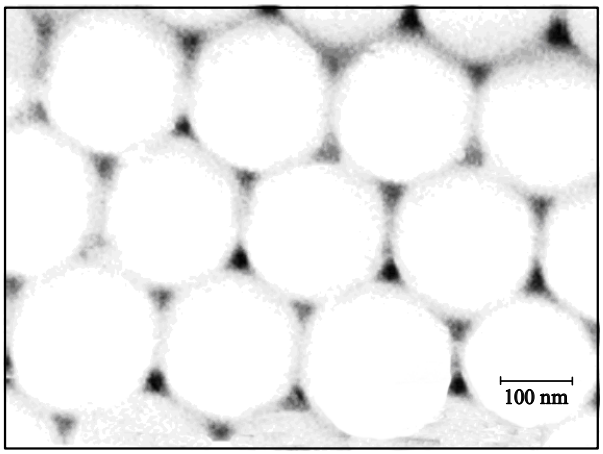

Figure 3. Electron-microscope photograph of artificial opals.

Voids in synthetic opals can occupy up to 26 % of the total volume (in the case of the point contact between amorphous SiO_2 globules). The size of voids (pores) is a few hundreds of nanometres, while the size of channels connecting pores is a few tens of nanometres. Pores contained in opal matrices can be filled with liquids wetting silica (Fig. 4).

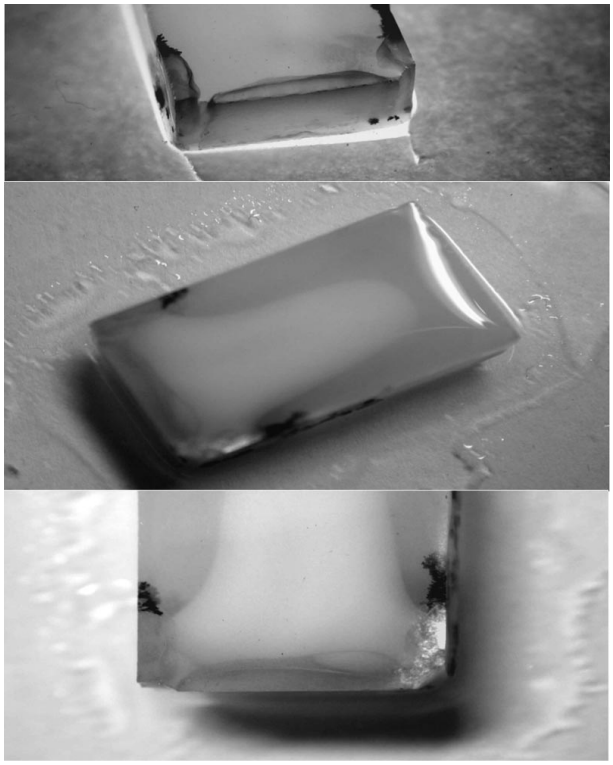

Figure 4. View of artificial opals filled with liquid.

In [25, 26], the optical properties of opals with voids filled with materials with high refractive indices n were studied. In this case, the optical contrast between the matrix and filler (the ratio of the refractive indices of the filler and amorphous SiO_2) considerably increases. It was shown in these papers that, by varying the degree of pore filling, the average dielectric constant of a composite can be changed in a broad range, thereby tuning the forbidden photonic band virtually over the entire visible (opal – GaN) and near-IR (opal – Si) ranges, the size of SiO_2 globules remaining the same. As fillers in globular photonic crystals, semiconductors with high refractive indices such as Si ($n \approx 3.5$), GaN ($n \approx 2.3$), etc. can be used. The modern technology of embedding these materials into porous structures allows the variation of the degree of opal-pore filling with semiconductors in a broad range. Therefore, a three-dimensional superlattice formed by particles of the filler can be produced in the opal structure (the size of clusters can vary from 10 to 400 nm). Upon filling pores in the crystal with various materials, fractal structures can be formed in which pores are filled only partially. The optical contrast can be further increased by inverting the structure of a composite material. The structure inversion involves the etching of SiO_2 from the initial opal – filler composite. As a result, a three-dimensional lattice is formed, which occupies up to 26 % of the composite volume and is located in the regular matrix of hollow globules occupying no less than 74 % of the volume.

3. On the theory of photonic bands in periodic structures

According to the general theory developed for periodic structures [27], for $a_0 = (2p+1)\lambda/2$ (λ is the wavelength and $p = 0, 1, 2, ...$), the corresponding wave interacting with a crystal lattice is reflected from the corresponding crystal plane. The interference of the incident and reflected waves gives rise to a standing wave. In this case, the propagation of particles with energies satisfying the Bragg condition proves to be impossible in an ideal crystal. In these spectral regions the forbidden bands are formed; the wave mechanism of their formation is common for all periodic structures.

In real crystals various phases can exist – regions with different lattice constants. Artificial globular photonic crystals grown based on natural compounds also can contain several coexisting phases. It is reasonable to analyse the structure of such crystals beginning from the simpler case of a single-phase photonic crystal.

By using the general theory of light propagation in superlattices [27], we consider the solutions of Maxwell's equation for a dielectric medium without free charges and currents simulating a photonic crystal. The system of Maxwell's equations in this case has the form

$$\begin{aligned} &\nabla \cdot \boldsymbol{D} = 0, \\ &\nabla \cdot \boldsymbol{B} = 0, \\ &\nabla \times \boldsymbol{E} = -\frac{\partial \boldsymbol{B}}{\partial t}, \\ &\nabla \times \boldsymbol{H} = \frac{\partial \boldsymbol{D}}{\partial t}. \end{aligned} \tag{1}$$

Here, $\boldsymbol{D} = \varepsilon\varepsilon_0\boldsymbol{E}$; $\boldsymbol{B} = \mu\mu_0\boldsymbol{H}$; and $[(\varepsilon_0\mu_0)^{-1}]^{1/2} = c_0$.

From (1), we obtain the relation

$$\varepsilon^{-1}(\boldsymbol{r})(\nabla \times \boldsymbol{H}) = \varepsilon_0 \frac{\partial \boldsymbol{E}}{\partial t}. \tag{2}$$

By applying the operator rot to the left- and right-hand sides of (2) and taking (1) into account, we obtain

$$\nabla \times \left[\varepsilon^{-1}(\boldsymbol{r})(\nabla \times \boldsymbol{H})\right] = -\frac{\mu}{c_0^2}\frac{\partial^2 \boldsymbol{H}}{\partial t^2}. \tag{3}$$

This gives the expression

$$\frac{\partial^2 \boldsymbol{H}(\boldsymbol{r}, t)}{\partial t^2} = -\omega^2 \boldsymbol{H}(\boldsymbol{r}, t) \tag{4}$$

for monochromatic waves.

For $\mu = 1$, we have

$$\nabla \times \left[\varepsilon^{-1}(\boldsymbol{r})(\nabla \times \boldsymbol{H})\right] = \left(\frac{\omega}{c_0}\right)^2 \boldsymbol{H}. \tag{5}$$

Because the quantity $\varepsilon(\boldsymbol{r})$ is real in the case under study, Eqn (5) is the problem for determining the eigenvalues of the quantity $(\omega/c_0)^2$ of the Hermitian operator $\hat{A} = \nabla \times [\varepsilon^{-1}(\boldsymbol{r})\nabla \times \boldsymbol{H}(\boldsymbol{r})]$ in the equation

$$\hat{A}\boldsymbol{H} = \left(\frac{\omega}{c_0}\right)^2 \boldsymbol{H}. \tag{6}$$

Consider a one-dimensional photonic crystal with the period $a = a_1 + a_2$, where a_1 and a_2 are the sizes of regions with dielectric constants ε_1 and ε_2, respectively. It is known that the eigenfunctions of Eqn (6) in a periodic structure have the Bloch form

$$\varphi = \exp(\mathrm{i}kx)u(x), \tag{7}$$

where x is the coordinate and k is the wave-vector modulus.

The eigenfunctions of the operator $\hat{A}$ can be found from (7) and boundary conditions described by the function

$$\varepsilon(x) = \begin{cases} \varepsilon_1, & pa \leqslant x < a_1 + pa, \\ \varepsilon_2, & a_1 + pa \leqslant x < (p+1)a, \end{cases} \tag{8}$$

where p is an integer. The eigenfunctions in regions with dielectric constants ε_1 and ε_2 have the form

$$\begin{aligned} \varphi_1(x) &= A\exp(\mathrm{i}k_1x) + B\exp(-\mathrm{i}k_1x), \\ \varphi_2(x) &= C\exp(\mathrm{i}k_2x) + D\exp(-\mathrm{i}k_2x), \end{aligned} \tag{9}$$

respectively, where A, B, C, and D are some coefficients.

Taking into account the continuity of the functions and their derivatives at the boundaries of drastic changes in the dielectric constant and the boundary conditions for the standing wave, we obtain the relations

$$\begin{aligned} &(A+B)\exp(\mathrm{i}ka) = \left[C\exp(\mathrm{i}ka) + D\exp(-ik_2a)\right], \\ &k_1(A-B)\exp(\mathrm{i}ka) = k_2\left[C\exp(\mathrm{i}k_2a) - D\exp(-\mathrm{i}k_2a)\right], \\ &A\exp(\mathrm{i}k_1a) + B\exp(-\mathrm{i}k_1a) = C\exp(\mathrm{i}k_2a) \\ &\quad + D\exp(-\mathrm{i}k_2a), \\ &k_1\left[A\exp(\mathrm{i}k_1a) - B\exp(-\mathrm{i}k_1a)\right] = k_2\left[C\exp(\mathrm{i}k_2a)\right. \\ &\quad \left. - D\exp(-\mathrm{i}k_2a)\right]. \end{aligned} \tag{10}$$

This system of equations for A, B, C, and D can be written in the matrix form

$$M(k_1, k_2, k)V = 0, \tag{11}$$

where

$$M(k_1, k_2, k) =$$

$$\begin{pmatrix} 1 & 1 & -\exp[\mathrm{i}d(k_2-k)] & -\exp[(-\mathrm{i}d(k_2+k)] \\ k_1 & -k_1 & -k_2\exp[\mathrm{i}d(k_2-k)] & k_2\exp[-\mathrm{i}d(k_2+k)] \\ \exp(\mathrm{i}k_1a) & \exp(-\mathrm{i}k_1a) & -\exp(\mathrm{i}k_2a) & -\exp(-\mathrm{i}k_2a) \\ k_1\exp(\mathrm{i}k_1a) & -k_1\exp(-\mathrm{i}k_1a) & -k_2\exp(\mathrm{i}k_2a) & k_2\exp(-\mathrm{i}k_2a) \end{pmatrix};$$

$$V = \begin{pmatrix} A \\ B \\ C \\ D \end{pmatrix}.$$

This system of equations has the nonzero solution if $\det M = 0$. By writing out the determinant, we obtain the dispersion law $\omega(k)$ in the explicit form:

$$\cos(k_1a_1)\cos(k_2a_2) - \frac{1}{2}\frac{\varepsilon_1+\varepsilon_2}{\sqrt{\varepsilon_1\varepsilon_2}}\sin(k_1a_1)\sin(k_2a_2) = \cos(ka), \tag{12}$$

where $k_i = \sqrt{\varepsilon_i}\,\omega/c_0$. Because $|\cos ka| \leqslant 1$, forbidden bands appear in the spectrum, i.e. the values of k for which the propagation of radiation in the crystal is impossible for

$$\left|\cos(k_1a_1)\cos(k_2a_2) - \frac{1}{2}\frac{\varepsilon_1+\varepsilon_2}{\sqrt{\varepsilon_1\varepsilon_2}}\sin(k_1a_1)\sin(k_2a_2)\right| > 1.$$

We proposed a one-dimensional model of a crystalline chain with additional bonds to analyse the band structure of a globular photonic crystal (Fig. 5). In this case, the role of oscillating particles is played by electrons contained in globules. The equation of motion for a chain of this type taking into account the interaction only between nearest neighbours has the form

$$m\ddot{u}(l) = -\gamma_0 u(l) - \gamma[2u(l) - u(l-1) - u(l+1)]. \tag{13}$$

Here, $u(l)$ is the displacement of the lth particle from the equilibrium position ($l = 0, 1, 2, \ldots$); γ_0 and γ are the elastic coefficients; and m are masses of oscillating particles. Taking into account that the solution of (13) is a plane monochromatic wave $u = u_0\exp[\mathrm{i}(kl - \omega t)$, we obtain the dispersion law

$$\omega^2(k) = \frac{\gamma_0}{m} + 4\frac{\gamma}{m}\sin^2\frac{ka}{2} \tag{14}$$

for the crystalline chain under study.

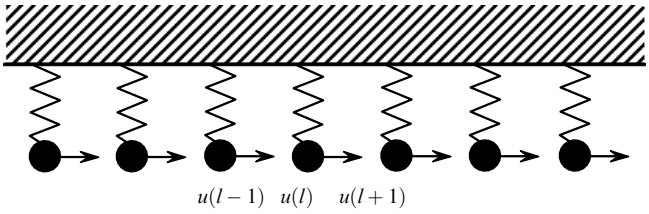

Figure 5. Monatomic chain with additional bonds.

If $\gamma_0 = 0$ and $\gamma > 0$, we obtain the dispersion law

$$\omega = 2\frac{S}{a}\sin\frac{ka}{2} \tag{15}$$

for the lowest branch (allowed band) of the photonic crystal, where $S^2 = \gamma a^2/m$. In this case, $S^2 = c_0^2/n_1 = c_1^2$, where c_0 is the speed of light in vacuum and n_1 is the effective refractive index. For the second and third photon branches, we have, respectively,

$$\omega^2 = \omega_{02}^2 - 4\frac{S_2^2}{a^2}\sin^2\frac{ka}{2}, \tag{16a}$$

where $\omega_{02}^2 = \gamma_{02}/m$; $S_2^2 = -\gamma a^2/m = c_2^2$; $\gamma = 0$, and

$$\omega^2 = \omega_{03}^2 - 4\frac{S_3^2}{a^2}\sin^2\frac{ka}{2}, \tag{16b}$$

where $\omega_{03}^2 = \gamma_{03}/m$; $S_3^2 = \gamma a^2/m = c_3^2$; and $\gamma = 0$.

At the boundary of the Brillouin zone, the frequencies of the lower and upper edges of the first forbidden photonic band are $\omega_1 = c_1\pi/a$, $\omega_2 = (\omega_{02}^2 - 4c_2^2/a^2)^{1/2}$, respectively.

The dependence of the group velocity $V_g = d\omega/dk$ on the wave vector for the branches under study can be obtained from the obtained dispersion laws for photonic bands. For the first, second, and third waves, we have

$$V_{g1} = c_1\cos\frac{ka}{2}, \tag{17}$$

$$V_{g2} = -\frac{c_2^2\sin ka}{\left[\omega_{02}^2a^2 - 4c_2^2\sin^2(ka/2)\right]^{1/2}}, \tag{18}$$

$$V_{g3} = \frac{c_3^2\sin ka}{\left[\omega_{03}^2a^2 + 4c_3^2\sin^2(ka/2)\right]^{1/2}}, \tag{19}$$

respectively.

It follows from relations (17)–(19) that near the forbidden-band edges ($k = \pi/a$) the group velocity of the corresponding electromagnetic waves tends to zero.

The dispersion law for photon branches in a real three-dimensional crystal is more complicated, in particular, due to the dependence of the frequency on the direction of the wave vector of the wave. In most artificial opals, the position of the forbidden photonic band depends on the wave-vector direction. In these cases, we are dealing with the so-called stop-band in the spectrum of the photonic crystal. The completely forbidden photonic band was obtained at present only for artificial opals with a high contrast ($\varepsilon_1 \gg \varepsilon_2$), in particular, for the so-called inverted opals, in which the initial opal matrix has been etched by preserving the filler structure. The presence of the stop-band in a globular photonic crystal leads to a strong reflection of light from the opal surface in this region. This results in a drastic decrease in the transmission of electromagnetic radiation in thin layers of the photonic crystal in the region of the stop-band upon illumination of the sample by a continuous spectrum.

To simplify calculations, we will assume that $\omega_{02} = \omega_{03} = \omega_0$ and $c_1 = c_2 = c_3 = c_0$. In this case, near the centre of the Brillouin zone (k tends to zero) we have for the three lower photonic bands:

$$\omega_1 = c_0k, \tag{20a}$$

$$\omega_2^2 = \omega_0^2 - c_0^2k^2, \tag{20b}$$

$$\omega_3^2 = \omega_0^2 + c_0^2k^2, \tag{20c}$$

respectively.

Thus, in a globular photonic crystal a photon can behave as in vacuum [relation (20a)], as a massive relativistic particle with the positive effective mass (20b), and as a quasi-particle with the negative effective mass (20c). For the dispersion law (20b), the sign of $d\omega/dk$ becomes negative.

Consider the situation when the angle of incidence of a light beam on the photonic-crystal surface is zero. Let us denote by $\boldsymbol{i}$ the direction of the unit vector of the normal to the crystal surface. Then, the velocity vector of a beam incident from vacuum on the crystal surface is $\boldsymbol{c}_0 = -c_0\boldsymbol{i}$. The direction of this vector coincides with that of the group-velocity vector inside the crystal and for $d\omega/dk < 0$, the directions of this vector is opposite to that of the phase-velocity vector $\omega\boldsymbol{i}/k$. In the case of the normal incidence, we have

$$\frac{\omega}{k}\boldsymbol{i} = \frac{\boldsymbol{c}_0}{n}. \tag{21}$$

Therefore, if $d\omega/dk$ is negative, it follows from (21) that the refractive index should also be negative. If $d\omega/dk > 0$, the phase- and group-velocity vectors coincide, and the refractive index should be positive. In any case, the relation

$$|n| = \frac{c_0k}{\omega(k)} \tag{22}$$

should take place, where $\omega(k)$ is the dispersion law of the corresponding wave.

In the approximation used here, according to (15) and (16), the first three bands are described by the relations

$$\omega_1(k) = \frac{2c_0}{a}\sin\frac{ka}{2}, \tag{23}$$

$$\omega_2(k) = \left(\omega_0^2 - 4\frac{c_0^2}{a^2}\sin^2\frac{ka}{2}\right)^{1/2}, \tag{24}$$

$$\omega_3(k) = \left(\omega_0^2 + 4\frac{c_0^2}{a^2}\sin^2\frac{ka}{2}\right)^{1/2}. \tag{25}$$

The spectral dependence of the reflection coefficient can be found from the known relation

$$R = \left|\frac{k - k_0}{k + k_0}\right|^2. \tag{26}$$

In this case, the dependences $k = k(\omega)$ are found from (22)–(25), and $k_0 = \omega/c_0$. The transmission coefficient (in the absence of losses) can be determined from the expression

$$T = 1 - \left|\frac{k - k_0}{k + k_0}\right|^2. \tag{27}$$

4. Experiments on the reflection of light from the surface of globular photonic crystals

The reflection spectra of opal matrices were analysed, in particular, in paper [14]. The measurements were performed by using the setup shown schematically in Fig. 6.

A light source was 100-W halogen incandescent lamp (*1*). The emission of the lamp was directed through lens collimator (*2*) to GS-5 goniometer (*3*) with an iris diaphragm at the exit slit. A sufficiently intense light beam of diameter 3 mm formed in this way was directed on opal sample (*4*) whose reflecting surface was located at the goniometer stage centre and was perpendicular to the stage plane. The divergence of the incident beam was no

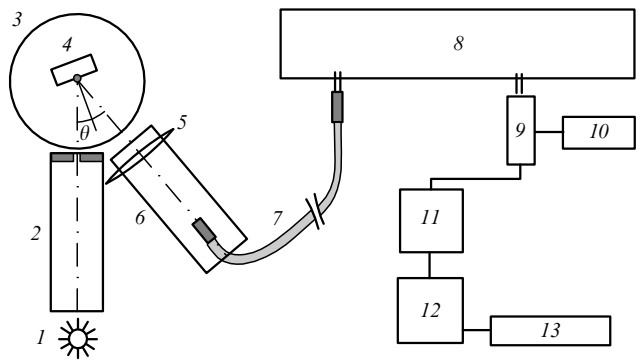

Figure 6. Scheme of the setup for measuring reflection spectra: (*1*) light source; (*2*) collimator; (*3*) GS-5 goniometer stage; (*4*) opal sample; (*5*) lens; (*6*) holder; (*7*) glass fibreoptic bundle; (*8*) DFS-12 monochromator; (*9*) FEU-79 photomultiplier; (*10*) power source; (*11*) analogue-to-digital converter; (*12*) computer; (*13*) printer.

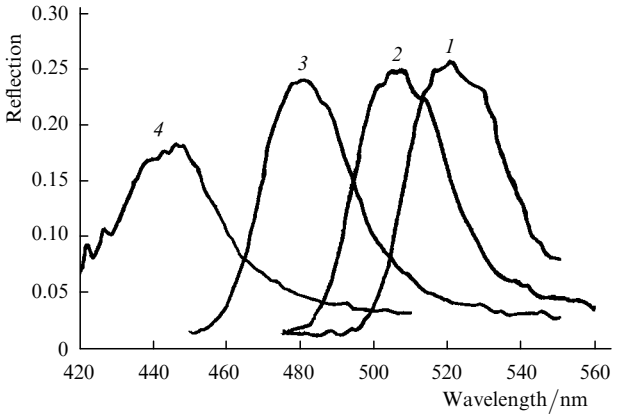

Figure 7. Reflection spectra of nominally pure photonic crystals for $\theta = 5^\circ$ (*1*), 20° (*2*), 30° (*3*), and 45° (*4*).

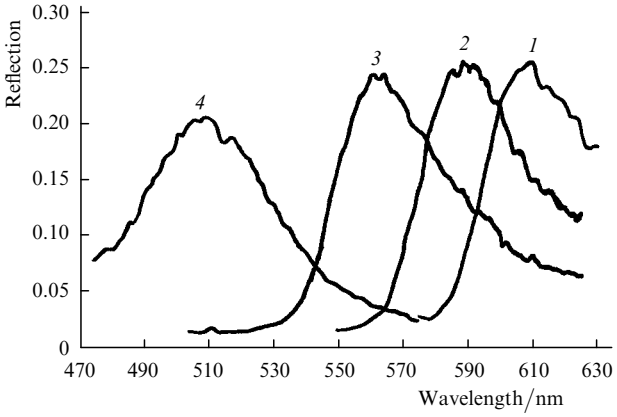

Figure 8. Reflection spectra of photonic crystals with voids between a-SiO_2 globules filled with a nonlinear $Ba(NO_3)_2$ material for $\theta = 5^\circ$ (*1*), 20° (*2*), 30° (*3*), and 45° (*4*).

more than 1′. The angle of incidence was varied by rotating the goniometer stage. The accuracy of measurement of the angle of incidence (reflection) was 5′. The reflected beam was projected on the end of a glass fibreoptic bundle of diameter 3 mm with the help of lens (*5*) of diameter 5 cm and focal distance 7 cm, which was located at the double focal distance from the sample and bundle end. In this way, both specular and diffusion components of the reflected light were collected. The second end of the fibreoptic bundle was located at the entrance slit of the monochromator of modified DFS-12 spectrometer (*8*) equipped with cooled FEU-79 photomultiplier (*9*) mounted at the exits slit of the monochromator. An analogue output signal of the photomultiplier was amplified, transformed to a digital signal by means of an analogue-to-digital converter, recorded, and was fed to a computer. Quantitative measurements were performed for angles $\theta = 5^\circ$, 20°, 30°, and 45°. To obtain the real spectra of light reflected from the surface of a photonic crystal, the intensity of the observed reflection spectrum was normalised to the intensity of the reflection spectrum of an aluminium mirror obtained under the same illumination conditions. This allowed us to exclude the influence of the monochromator (the spectral dependence of the reflectivity of a diffraction grating) and the spectral sensitivity of the photomultiplier and to obtain the absolute values of the reflection coefficient.

In [14], opal samples of size $1 \times 0.5 \times 0.5$ cm consisting of monodisperse spherical a-SiO_2 particles were investigated. According to [14], the FCC lattice is formed in such opals. The samples were filled with a dielectric by impregnating pure opals with a saturated alcohol solution of barium nitrate followed by the evaporation of ethyl alcohol by heating in air up to 150 °C during an hour. Then, the sample was annealed by using a 1-W repetitively pulsed copper vapour laser. The spectra of reflection from the growth (111) plane were measured both for pure crystals (sample no. 1) and crystals with voids between a-SiO_2 particles filled with a nonlinear-optical $Ba(NO_3)_2$ material (sample no. 2).

The reflection bands obtained in [14] are asymmetric and depend on the angle of incidence (Figs 7 and 8). The reflection maximum for sample no. 1 was observed at the wavelengths 506, 482, and 446 nm for the angles of incidence of 20°, 30°, and 45°, respectively, while for sample no. 2 – at the wavelengths 590, 564, and 510 nm, respectively. The reflection coefficient for the angle of incidence of 20° was 25 % for both samples. As the angle of incidence of light was increased, the broadening of the reflection band was observed. Thus, the bandwidth was ~30 nm for angles 20° and 30°, while for the angle 45°, it was 36 nm. The red shift of the reflection band for sample no. 2 compared to the position of the reflection band of the unfilled opal (sample no. 1) for the same angles of incidence is explained by a change in the refraction index in pores of the opal matrix caused by their filling with barium nitrate.

The reflection spectra were analysed in [14] by using the known expression $\lambda(\theta) = 2a(\langle n\rangle^2 - \sin^2\theta)^{1/2}$ for the Bragg diffraction of light in opals, where $a = \sqrt{2/3}d$ is the distance between planes in the crystal; θ is the angle of incidence of a light beam on the crystal; $\langle n\rangle = \beta n_1 + (1-\beta)n_2$ is the effective refractive index for synthetic opal; β is the filling factor for SiO_2 globules; n_1 and n_2 are the effective refractive indices of silica and the filler material, respectively. The dependence of the wavelength of the reflection maximum on the angle of incidence was calculated from this expression. The values of physical parameters used for sample no. 1 were $n_1 = 1.47$, $n_2 = 1$, $\beta = 0.74$, and $d = 230$ nm. The diameter of globules was calculated by the spectra of the normal reflection ($\theta = 5^\circ$). The wavelengths of the reflection maxima calculated for $\theta = 20^\circ$, 30°, and 45° were 505, 482, and 444 nm, respectively. The values of physical parameters used for sample no. 2 were $n_1 = 1.47$, $n_2 = 1.57$ [$Ba(NO_3)_2$],

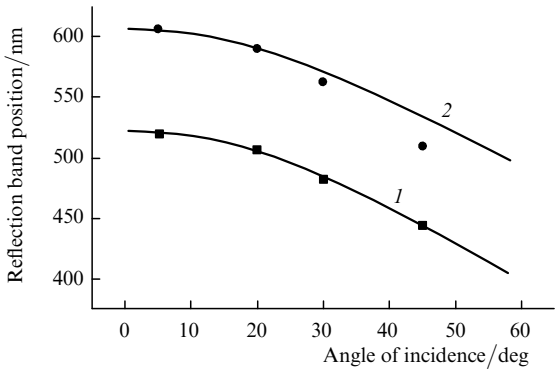

Figure 9. Angular dependences [14] of the positions of specular reflection bands for artificial opal samples nos 1 (*1*) and 2 (*2*). The curves are calculations, and points are experiment.

$\beta = 0.74$, and $d = 230$ nm. The wavelengths of the reflection maxima calculated for $\theta = 20^\circ$, 30°, and 45° were 590, 571, and 534 nm, respectively. For sample no. 1, the experimental and calculated wavelengths of the reflection maxima are in good agreement, while for sample no. 2 the discrepancy between the theory and experiment is quite large [see curves (*1*) and (*2*) in Fig. 9]. This is probably related to the specific features of pore filling.

The width of the reflection bands is mainly determined by the width of the stop-band and is 30, 30, and 36 nm for the angles of incidence 20°, 30°, and 45°, respectively, for sample no. 1. For sample no. 2, the bandwidth is 50, 50, and 57 nm for the same angles of incidence, respectively. The broadening of the reflection bands and a decrease in the reflection coefficient with increasing angle of incidence can be caused by light scattering by defects of synthetic opal. The increase in the width of the reflection bands in filled opal is probably caused by filling defects. Among these effects can be growth twins, the deviations from the [111] orientation in some blocks (domains) forming opal [5], and structural defects of blocks themselves and their boundaries.

Figure 10 shows the spectral dependence of the reflection coefficient R obtained for a light beam nearly normally incident on the (111) surface [14].

The spectral dependences of the reflection coefficient were calculated by expression (26) by selecting parameters to provide the agreement with the experimental data. Figure 11 shows the theoretical spectral dependence of the reflection coefficient for a light beam normally incident on the (111)

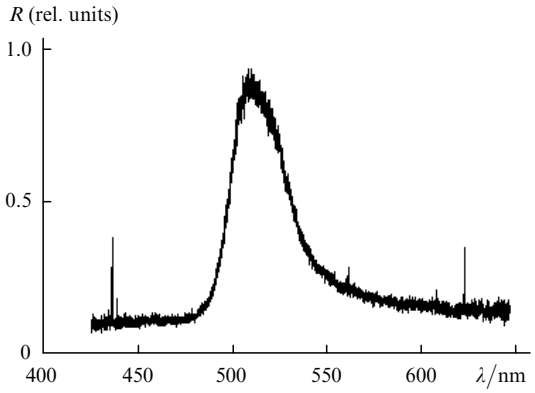

Figure 10. Experimental spectral dependence of the coefficient of reflection from the (111) surface for a small angle of incidence.

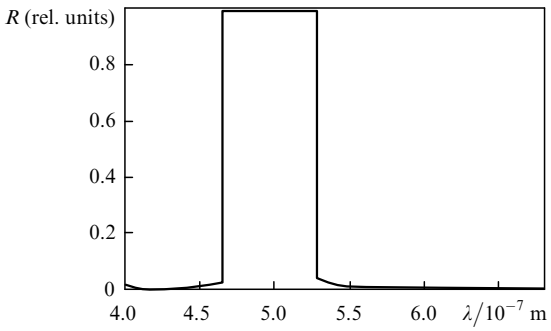

Figure 11. Theoretical spectral dependence of the reflection coefficient for a bean normally incident on the (111) surface of the initial opal.

surface of unfilled opal calculated for $\omega_{02} = \omega_{03} = 5.39 \times 10^{15}$ rad s^{-1} and $a = 1.68 \times 10^{-7}$ m [14]. One can see that the experimental and theoretical dependences in Figs 10 and 11 are in qualitative agreement, although the curves have considerably different shapes. The latter circumstance can be explained by the decay of electromagnetic waves and the influence of crystal-lattice defects. The reflection spectra give the boundaries of the stop-band for a beam normally incident on the (111) surface of the opal matrix: $\lambda_1 = 480$ nm (the upper bound) and $\lambda_2 = 520$ nm (the lower bound).

Curves (*1–3*) in Figure 12 from paper [17] show the corresponding dispersion curves for the condition $c_1 = c_2 = c_3 = c_0$.

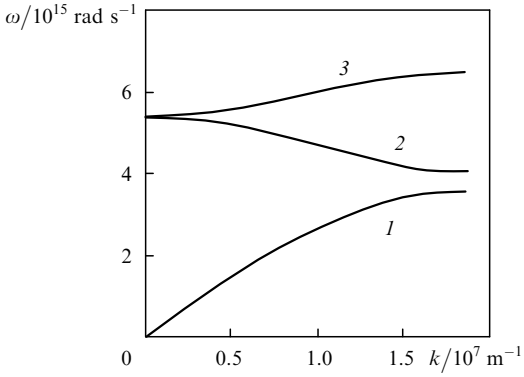

Figure 12. Dispersion branches (*1–3*) for the photonic crystal under study.

Thus, experiments on the reflection of light from the surface of bulk opal matrices allow one to determine the basic parameters of photonic bands and estimate the size of globules from which the opal matrix is formed. Note also here that real photonic crystals should be expected to contain numerous defects related to a change in the orientation of domains and other features of the crystal growth. This conclusion is confirmed both by high-spatial resolution experiments on the reflection of light from the surface of opals and experiments [13] on the reflection of the shorter-wavelength radiation from opal matrices. The presence of defects in real opal matrices is demonstrated by digital 1000x microscopic images of the surface of opals illuminated by a continuous visible light (Fig. 13). One can see from these photographs that the size of defects near the

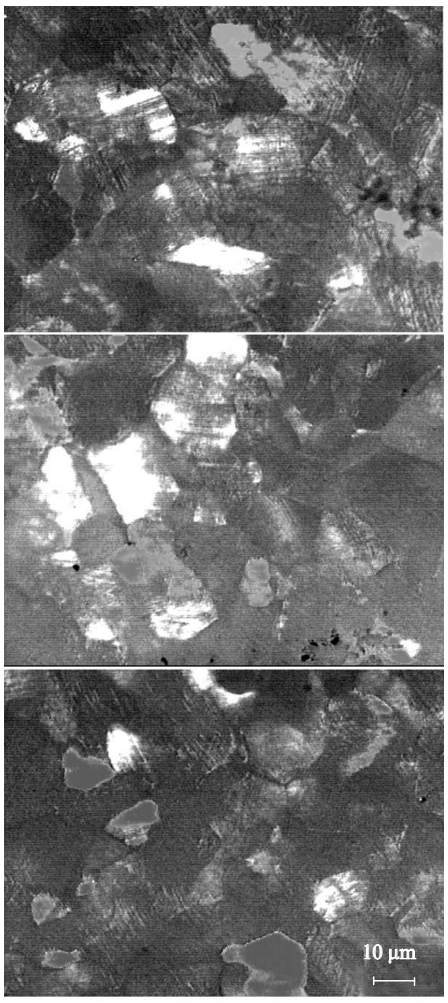

Figure 13. Microphotographs of different regions of the photonic crystal surface obtained by using a digital camera of an optical microscope. Different regions correspond to the manifestation of microscopic defects on the surface.

surface of the opal matrix, which change the colour of light reflected from the surface, is a few tens of micrometres. The number of defects in the crystal lattice of opal matrices can be reduced by improving the technology of their growth.

5. Group velocity of electromagnetic waves and the effective photon mass in a globular photonic crystal

The group velocity $V_g = d\omega/dk$ of electromagnetic waves can be calculated if the dispersion law for photon branches is known. We have

$$V_{g1} = c_0 \sin\frac{ka}{2}, \tag{28}$$

$$V_{g2} = -\frac{c_0^2 \sin(ka/2)\cos(ka/2)}{\left[\omega_0^2 a^2 - 4c_0^2 + 4c_0^2\cos^2(ka/2)\right]^{1/2}}, \tag{29}$$

$$V_{g3} = \frac{2c_0^2 \sin(ka/2)\cos(ka/2)}{\left[\omega_0^2 a^2 + 4c_0^2 - 4c_0^2\cos^2(ka/2)\right]^{1/2}} \tag{30}$$

for the first, second, and third photon branches.

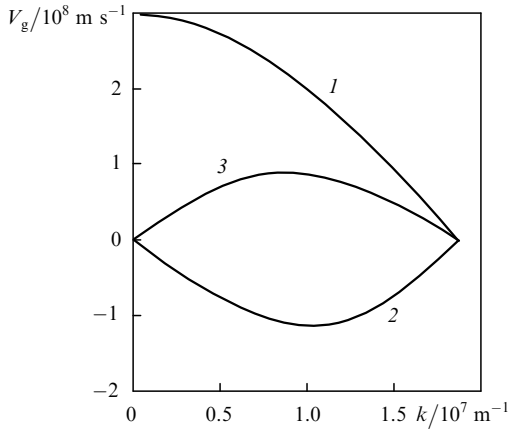

Figure 14. Dependences of the group velocity on the wave vector for the first (*1*), second (*2*), and third (*3*) lower photon branches.

Figure 14 presents the dependences of the group velocity on the wave vector calculated for $\omega_0 = 5.39 \times 10^{15}$ rad s^{-1} and $a = 1.68\times 10^{-7}$ m. One can see that is positive for the first and third photon branches, while the value of $d\omega/dk$ for the second photon branch is negative.

It follows from Fig. 14 that the photon velocity (the group velocity of the corresponding electromagnetic waves) becomes very small near the Brillouin zone boundary and at the zone centre. The corresponding electromagnetic excitations were called slowtons. The photon state density is inversely proportional to the group velocity [28]. Therefore, the probability of generation of slowtons in various processes (emission of impurity atoms or molecules, parametric and Raman scattering of light, generation of optical harmonics), which is proportional to the density of final states, should increase when the edge of the stop-band is approached.

The dependence of the effective photon mass in a globular photonic crystal on the wave vector was calculated in [17] by using the known relations for the effective mass of quasi-particles

$$\mu = h\left(2\pi\frac{d^2\omega}{dk^2}\right)^{-1}, \tag{31}$$

where h is Planck's constant.

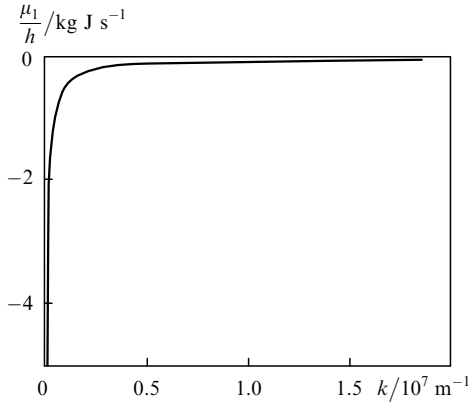

Figure 15. Dependence of the effective photon mass μ_1 on the wave vector for the first photon branch.

For the first and photon branch, the dependence

$$\mu_1 = -\frac{h}{\pi c_0 a \sin(ka/2)} \tag{32}$$

was obtained (Fig. 15).

For the second photon branch, the dependence has the form (Fig. 16)

$$\mu_2 = -\frac{ha\left[\omega_0^2 a^2 - 4c_0^2 \sin^2(ka/2)\right]^{1/2}}{2\pi\left[4c_0^4\omega^{-2}\cos^2(ka/2)\sin^2(ka/2) + c_0^2 a^2 \cos^2(ka/2) - c_0^2 a^2 \sin^2(ka/2)\right]}. \tag{33}$$

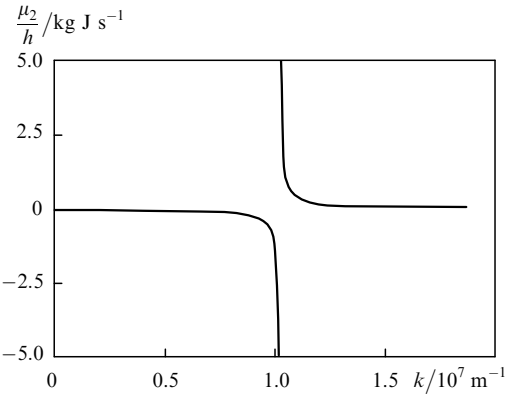

Figure 16. Dependence of the effective photon mass μ_2 on the wave vector for the second photon branch.

And for the third photon branch, we have (Fig. 17)

$$\mu_3 = -\frac{ha\left[\omega_0^2 a^2 + 4c_0^2 \sin^2(ka/2)\right]^{1/2}}{2\pi\left[4c_0^4\omega^{-2}\cos^2(ka/2)\sin^2(ka/2) - c_0^2 a\, 2\cos^2(ka/2) + c_0^2 a^2 \sin^2(ka/2)\right]}. \tag{34}$$

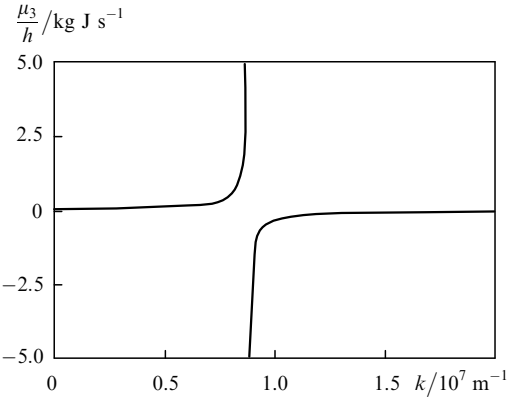

Figure 17. Dependence of the effective photon mass μ_3 on the wave vector for the third photon branch.

6. Dispersion of the refractive index in a globular photonic crystal

By using (21), we obtain the relation

$$\frac{\omega}{k}\frac{\boldsymbol{k}}{k} = \frac{\boldsymbol{c}_0}{n}. \tag{35}$$

Here, the direction of the wave vector $\boldsymbol{k}$ coincides with the direction of the phase-velocity vector, while the direction of the vector $\boldsymbol{c}_0$ specifies the direction of the group velocity V_g of an electromagnetic wave inside a globular photonic crystal. Thus, if the directions of the group- and phase-velocity vectors coincide, the refractive index is positive. If these directions are opposite, the refractive index is negative. Figure 18 shows the frequency dependences of the refractive index for all the three photon branches obtained in [17]. The dependences exhibit anomalies near the points corresponding to the Brillouin-zone edges.

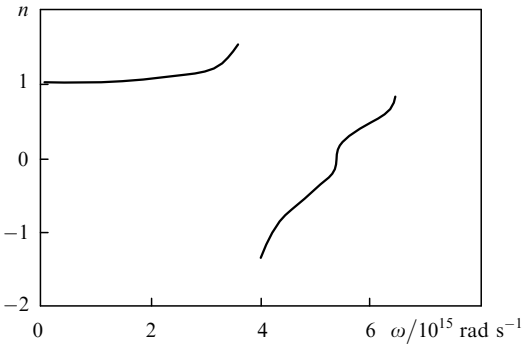

Figure 18. Dispersion of the refractive index in a photonic crystal.

7. Bound photon states in globular photonic crystals

At the first stage of analysis of the properties of various elementary excitations (quasi-particles), the interaction between them is neglected. At the second stage, the interaction between quasi-particles resulting in their attraction or repulsion is considered. In the case of attraction between particles, the bound two-particle or, generally, many-particle states can be formed. If a bound two-particle state is short-lived, we are dealing with the so-called resonances. In the case of a long-lived bound two-particle state, we are dealing with a bound state corresponding to a new quasi-particle.

The properties and conditions of existence of the bound states of two phonons, magnons, plasmons, and rotons, which are Bose particles, were earlier investigated in detail. It was established, in particular, that conditions for the binding of quasi-particles are fulfilled in the case of the Fermi resonance, when the bound-state energy is close to the energy of fundamental excitations of the same symmetry type. Another important condition for the binding of quasi-particles even in the presence of a weak attraction between them is the anomaly of the density of states in the region of energies of free particles. A special case corresponds to the binding of Fermi quasi-particles, for example, electrons into pairs. In this case, the so-called Cooper pairs are produced, which play an important role in superconductivity.

The author of this review considered in [20] the possibility of formation of biphotons – a bound state of photon pairs with a finite mass in a globular photonic crystal. The theoretical analysis of the conditions for formation of biphotons is based on the general theory of the bound states of pairs of quasi-particles, developed earlier.

As the elementary excitations of electromagnetic waves involved in the formation of the bound photon states, photons with a finite effective mass interacting with each other were considered. The Hamiltonian for such quasi-particles can be written in the form

$$H = \sum_k E_k a_k^+ a_k + g_4 \sum_{k,p,q} a_{k+q}^+ a_{p-q}^+ a_p a_k + \dots . \tag{36}$$

Here, E_k is the photon energy; a_k and a_k^+ are the photon annihilation and creation operators, respectively; and g_4 is the parameter characterising the interaction between quasi-particles caused by the photon – photon anharmonicity and corresponding to four-particle scattering in a real crystal (the dependence of g_4 on the wave vector of quasi-particles is neglected for simplicity).

The problem is solved in this approximation by summing the Feynman diagrams corresponding to the elementary processes of photon – photon scattering in a material medium.

By summing the Feynman diagrams for four-particle processes (Fig. 19), we obtain the Bethe – Salpeter equation, whose solution has the form

$$G_2(Q,\omega) = \frac{G_{02}(Q,\omega)}{1 - g_4 G_{02}(Q,\omega)}, \tag{37}$$

where

$$G_{02}(Q,\omega) = \int \frac{\rho_{02}(Q,\omega)\mathrm{d}E}{\omega - E + 2\mathrm{i}\gamma}; \tag{38}$$

and $\rho_{02}(Q,\omega)$ is the density of two-photon states of free quasi-particles. This quantity becomes anomalously high when the velocities of the particles are anomalously small. In particular, as follows from analysis of the dependences of group velocities on the wave vector, such a situation takes place for slowtons corresponding to the regions near the Brillouin-zone edges. If the condition

$$1 = g_4 G_{02}(Q,\omega) \tag{39}$$

is fulfilled, then for $g_4 > 0$, the bound state can be stable even in the case of weakly interacting quasi-particles.

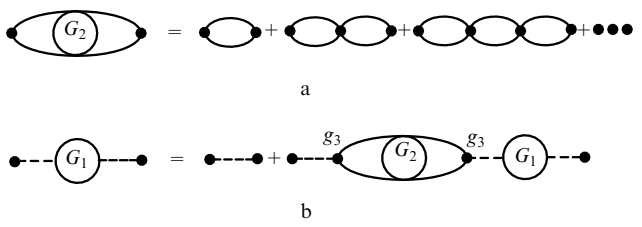

Figure 19. Feynman diagrams corresponding to four-particle (a) and three-particle (b) processes; G_1 and G_2 are the single-particle and two-particle Green functions.

The spectrum of bound states is described by the expression

$$\rho_2(Q,\omega) = -\frac{\mathrm{Im}\, G_2(Q,\omega)}{\pi}. \tag{40}$$

Consider now the situation when excited states exist in the material medium of a globular crystal, the corresponding irreducible representations of these states belonging to the reducible representation of the second-rank tensor. In particular, in the presence of the inversion centre in the point symmetry group of the medium, such representations can be even symmetry types A_g, E_g, etc. One-photon transitions from such excited states to the ground state are forbidden by the selection rules. For this reason, it is reasonable to call such states the dark (darkton) states and the corresponding particles – darktons. Examples of darktons are optical phonons classified by the even symmetry types. Such phonons appear, according to the selection rules, in two-photon processes, in particular, upon spontaneous or stimulated Raman scattering in centrally symmetric molecules or crystals. Another example of such excitations is mechanical oscillations of globules, in particular, 'breathing' oscillations. Finally, the even two-electronic states can exist in the UV region in organic and inorganic structures. In this case, the model Hamiltonian can be written in the form

$$H = \sum_k E_k a_k^+ a_k + g_3 \sum_{k,q} d_k^+ a_q a_{k-q} + \mathrm{H.c.} \tag{41}$$

Here, d_k^+ and d_k are the darkton creation and annihilation operators, respectively; and g_3 is the parameter characterising three-particle interaction processes.

If only three-particle processes are taken into account ($g_4 = 0$), it is necessary to sum up diagrams corresponding to the Dyson equation. In this case, we obtain

$$G_1(\omega) = \frac{G_1^0}{1 - g_3^2 G_1^0 G_2^0(Q,\omega)}, \quad G_1^0 = \frac{1}{\omega - \omega_0 - \mathrm{i}\gamma}. \tag{42}$$

It follows from this that a bound state appears if

$$1 = g_3^2 G_1^0 G_2^0(Q,\omega). \tag{43}$$

Such a situation takes place if the analogue of the Fermi resonance is realised, i.e. if in the energy region of the two-particle state a real state with the symmetry of the two-photon state is present. Because photons are vector particles, the transformation properties of the two-photon state are characterised by the second-rank tensor. The wave functions of such a state in structures with the inversion centre are even with respect to the inversion operation and are classified by the even types of symmetry. Thus, bound states are formed in centrally symmetric structures when the darkton-state energy in a crystal is close to that of two free photons. The bound states of two photons in this case are one of the types of darkton states. In a real photonic crystal, the bound states can be formed due to three-particle and four-particle interactions.

It is important to note that the formation of the bound state of two photons in centrally symmetric structures is

accompanied by the production of biphotons whose symmetry considerably differs from that of initial quasiparticles: while photons are classified according to their transformation properties as vector particles, photons bound in pairs are classified by the second-rank tensor. Thus, bound photon pairs of the scalar or pseudo-scalar (axial) type can exist in a centrally symmetric medium. The properties of biphoton radiation in centrally symmetric media should considerably differ from usual electromagnetic waves. In particular, this radiation should be invisible and should penetrate through material media without considerable absorption.

8. Single-photon-excited delayed scattering of light in globular photonic crystals exposed to cw UV radiation

Opal matrices consisting of a-SiO_2 globules have fundamental absorption only in the far-UV region. The secondary emission spectra in fused silica were investigated earlier upon excitation by short-wavelength radiation due to a broad energy gap of silica. The KV silica samples excited in the mid-UV region at 255.3 nm exhibit weak luminescence bands at 300 and 390 nm. Thus, the luminescence of pure opals excited by visible or near-UV radiation should be very weak. This does not exclude, however, the possibility of observing secondary emission caused by various processes such as Raman scattering, photoluminescence, three-photon parametric scattering, four-photon parametric scattering (upon pulsed laser excitation), stimulated scattering of light, multiphoton excitation, etc. We studied such effects by analysing secondary emission in various opal matrices excited by different radiation sources.

At the first stage, we investigated the features of secondary emission in initial (unfilled) opals excited by incoherent radiation from semiconductor light-emitting diodes (LEDs). Artificial opal plates of thickness 0.7 and 2.0 mm and sides $\sim$10 mm cut out along the [111] direction were used. The energy of the forbidden photon band was determined in experiments on specular reflection of broadband radiation from samples. We found that the forbidden band (stop-band) upon the normal incidence of light was in the range between 480 and 520 nm, corresponding to the globular diameter $d = 230$ nm.

Secondary emission was excited by the 30–40-mW radiation from semiconductor LEDs at 363.5 and 381.5 nm with a bandwidth of 10 nm. In this case, photoluminescence of amorphous silica in artificial opals was virtually absent.

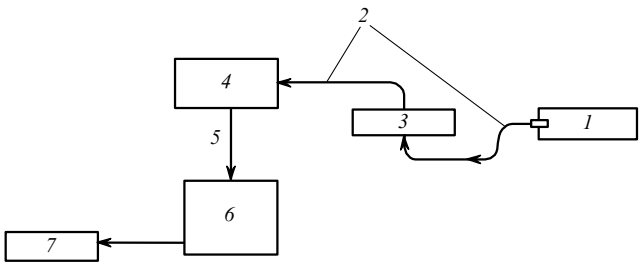

Figure 20. Setup for analysis of secondary emission in artificial opals; (*1*) excitation source; (*2*) silica fibre; (*3*) sample; (*4*) minipolychromator; (*5*) cable; (*6*) computer; (*7*) printer.

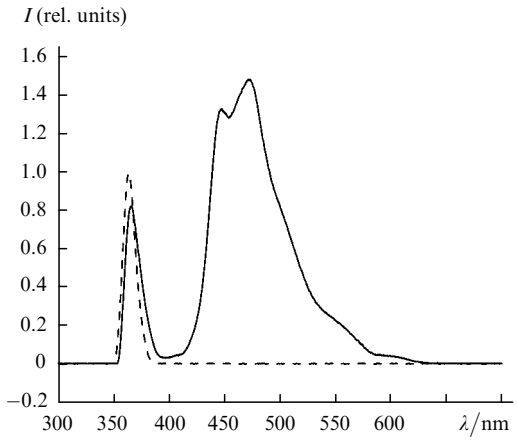

Figure 21. Emission spectrum of a 0.7-mm thick opal plate excited by a LED at 365.3 nm. The dashed curve is the spectrum of exciting radiation.

Figure 20 shows the scheme of the experimental setup used in [22] to analyse the secondary emission spectra observed upon continuous UV excitation. Radiation from a LED was directed through a fibre of diameter 2 mm to the surface of opal plates of thickness 0.7 and 2.0 mm. Secondary emission was collected from the surface opposite to the illuminated one with the help of a silica fibre with the fibre core of diameter 200 μm and directed through this fibre to a miniature FSD8 polychromator, the output end of the fibre being used as the entrance slit of the polychromator. The emission spectrum was recorded with a CCD linear array used with the polychromator.

The optical and spectral characteristics of the polychromator provided a high sensitivity of the method. The emission spectra of opals were recorded in our experiments [22] for 0.1–10 s.

Figure 21 shows the secondary emission spectrum of a 0.7-mm-thick artificial opal plane–parallel plate excited by a UV LED at 363.5 nm. The spectrum exhibits two maxima at 447.3 and 472.4 nm, the emission intensity is approximately two orders of magnitudes lower than that of the exciting radiation.

Figure 22 presents the secondary emission spectrum of a 2.0-mm-thick opal plate excited at 363.5 nm. One can see

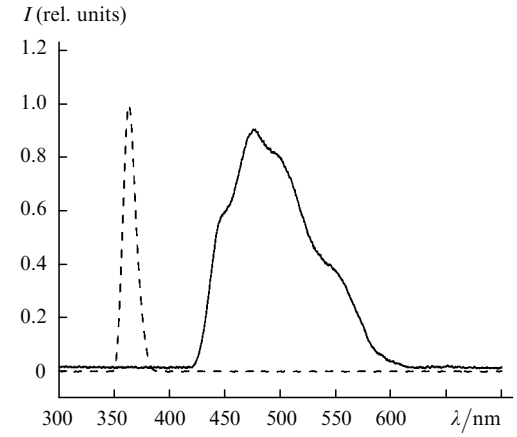

Figure 22. Emission spectrum of a 2.0-mm thick opal plate excited by a LED at 365.3 nm. The dashed curve is the spectrum of exciting radiation.

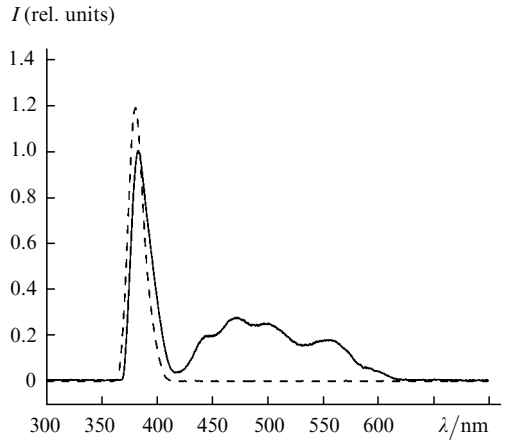

Figure 23. Emission spectrum of a 0.7-mm thick opal plate excited by a LED at 381.5 nm. The dashed curve is the spectrum of exciting radiation.

that in this case the emission band is broader and its maximum shifts to 477.7 nm. No emission in the high-frequency region was observed. Figure 23 presents the secondary emission spectrum of the 0.7-mm-thick opal plate excited at 381.5 nm, and Fig. 24 illustrates the emission spectrum of the 2.0-mm-thick opal plate. One can see from the spectra presented in Figs 21 – 24 that the width of the emission band for the given thickness of a sample increases when the excitation wavelength changes from 363.5 to 381.5 nm.

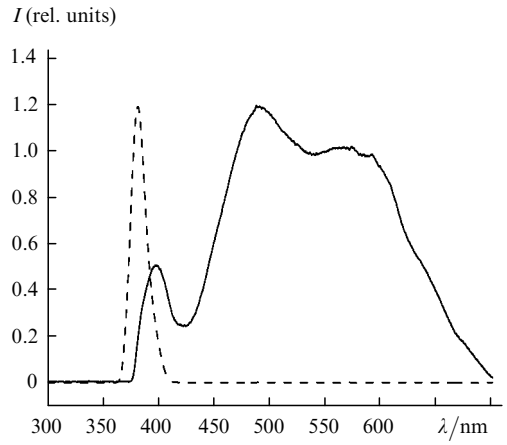

Figure 24. Emission spectrum of a 2.0-mm thick opal plate excited by a LED at 381.5 nm. The dashed curve is the spectrum of exciting radiation.

Figures 25 and 26 show the secondary emission spectra for opal plates of thickness 0.7 and 2.0 mm excited at 363.5 and 381.5 nm, respectively [22]. One can see that for the given excitation wavelength the emission band shifts to the red in a thicker sample, which illustrates efficient reemission inside this sample.

Let us analyse secondary emission spectra observed in unfilled artificial opals excited by UV radiation. The low-frequency band observed near the 381.5-nm excitation band appears due to spontaneous Stokes Raman scattering.

It is important that the intensity of the Stokes Raman band is comparable in this case with that of exciting radiation. This effect can be treated as Raman opalescence,

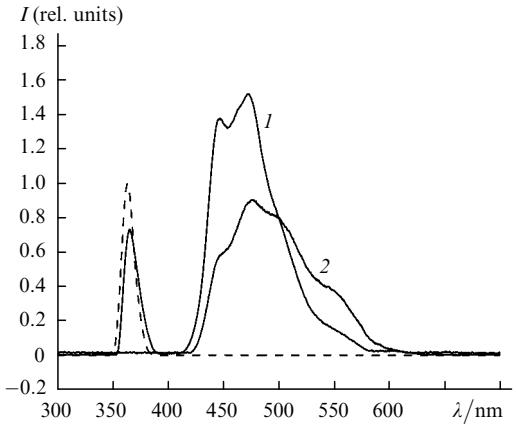

Figure 25. Emission spectra of a 0.7-mm thick (*1*) and 2.0-mm (*2*) thick opal plates excited by a LED at 365.3 nm. The dashed curve is the spectrum of exciting radiation.

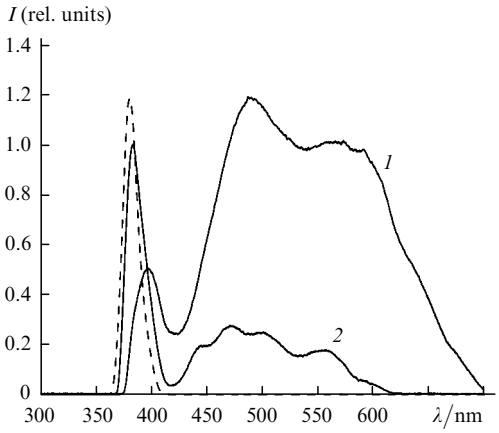

Figure 26. Emission spectra of a 0.7-mm thick (*1*) and 2.0-mm (*2*) thick opal plates excited by a LED at 381.5 nm. The dashed curve is the spectrum of exciting radiation.

i.e. a drastic increase in the probability of the Raman process. This can be explained by the proximity of the excitation band to the photon-band edge and, hence, to the maximum of the density of photons states In this case, the velocity of the electromagnetic wave becomes considerably lower than the speed of light c_0 in vacuum, i.e. $c_0/V_g \gg 1$. Correspondingly, the light-energy density and the alternating electric field inside a sample increase, resulting in the increase in the probability of Raman processes.

Numerous scattering centres of size close to the excitation wavelength contained in artificial opal also can enhance the intensity of Raman scattering. This leads to the resonator effect, the diffusion motion of photons, and the increase in their path in a sample.

Of special interest is the explanation of the secondary emission band located away from the excitation band in the case when Raman processes should not affect substantially the emission spectrum of opal in the long-wavelength (Stokes) spectral region. The secondary emission in this region can be explained by three-photon parametric scattering of light in which a UV photon is decomposed in the elementary event into one visible photon and one IR photon. In bulk centrally symmetric crystals, such processes are forbidden by the known selection rules. However, in our

case the selection rules corresponding to the centrally symmetric structure are invalid due to porosity of a photonic crystal because the crystal structure is noncentral near the crystal surface. The three-photon parametric light scattering is usually observed in anisotropic noncentral structures for which the known synchronism condition – the quasi-momentum conservation law, can be fulfilled. The law of conservation of energy and the synchronism condition in the elementary parametric process have the form

$$\omega_0 = \omega_1 + \omega_2, \qquad \boldsymbol{k}_0 = \boldsymbol{k}_1 + \boldsymbol{k}_2 + \boldsymbol{b}_i. \tag{44}$$

where $\boldsymbol{b}_i$ is the reciprocal lattice vector ($i = 1, 2, 3$).

Due to the presence of this vector, the synchronism condition proves to be fulfilled for several directions in a crystal, which simplifies the observation of such scattering in artificial opals. Another factor leading to the loss of directivity of parametric scattering in a globular photonic crystal is a strong inhomogeneity caused by the presence of numerous domains in the crystal. Excitation is performed by UV photons with frequency ω_0. One of the photons (with frequency ω_2) produced in three-photon parametric scattering corresponds to the blue–green spectral region. In this region, the forbidden photon band is located as well as regions of a drastic increase in the density of photon states near the forbidden-band edges and a drastic slowing down of the group velocity of the corresponding electromagnetic waves. Thus, the photon with frequency ω_1 is a slow photon – a slowton. The frequency ω_2 of a photon produced in the elementary scattering event lies in the IR spectral range.

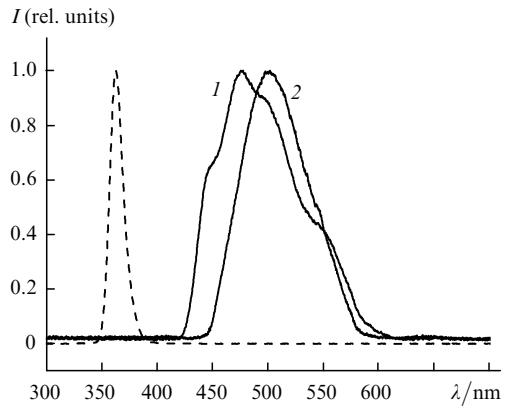

Figure 27. Emission spectra of pure opal (*1*) and opal filled with stilbene (*2*) and excited by UV radiation. The dashed curve is the spectrum of exciting radiation.

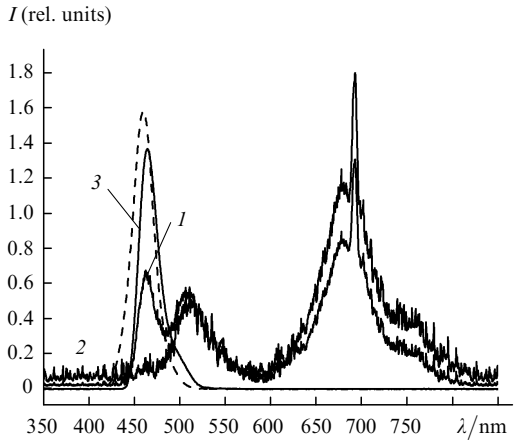

Figure 28. Emission spectra of opal filled with POPOP at a lower (*1*) and higher (*2*) concentration; (*3*) photoluminescence spectrum. The dashed curve is the spectrum of exciting radiation.

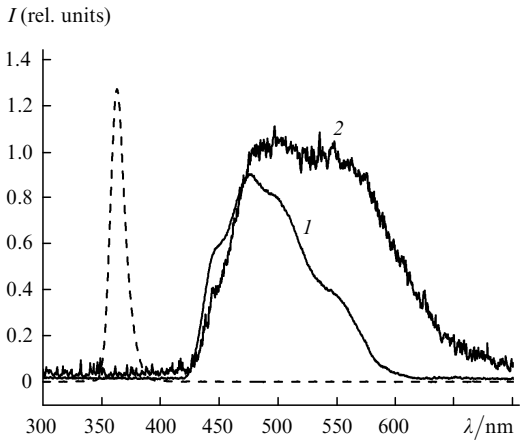

Figure 29. Emission spectra of initial opal (*1*) and opal filled with sodium nitrite (*2*). The dashed curve is the spectrum of exciting radiation.

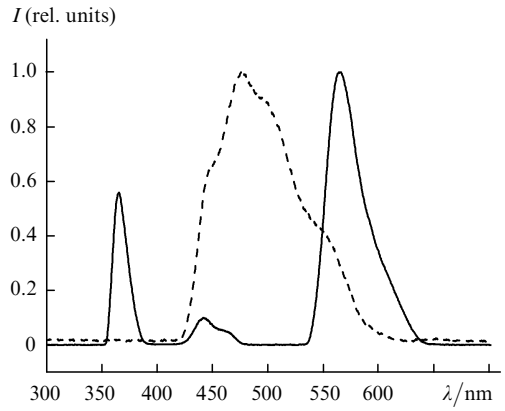

Figure 30. Emission spectra of opal filled with silver nanoparticles (solid curve). The dashed curve is the spectrum of exciting radiation.

Because the elementary processes of spontaneous Raman and three-photon parametric scattering result in the appearance of slowtons, scattering of this type can be called single-photon-excited delayed scattering.

To specify the nature of the observed secondary emission, we performed additional experiments [21] with samples filled with various dielectrics: organic compounds with the centrally symmetric structure [stilbene (Fig. 27) and POPOP (Fig. 28)] and inorganic compounds with the symmetry group containing both the inversion centre (rhombic sulphur) and belonging to noncentrally symmetric structures [sodium nitrite (Fig. 29), ammonium dihydrophosphate, triglycine sulphate).

In addition, we performed experiments with opal matrices filled with gold or silver particles (Fig. 30) [21]. In particular, an opal matrix was impregnated with an

aqueous colloidal silver suspension and then dried by heating up to 100 °C.

We found that the emission spectrum of opal matrices filled with stilbene, whose fluorescence spectrum is located in the near-UV region, shifted to the Stokes region. This can be explained by the shift of the forbidden band (stop-band), which is similar to the shift of the reflection maximum of light in opals filled with barium nitrate. The same situation was observed for opals filled with crystalline sulphur. A more complicated picture was observed for opals filled with the known POPOP luminophore (Fig. 28). The fluorescence spectrum of POPOP excited by UV diodes is located in the blue region. At the initial stage of filling of the opal matrix with POPOP, the POPOP fluorescence intensity deceased and two new secondary emission bands appeared. These bands can be related to emission from the lower and upper edges of the forbidden band. As the opal matrix was further filled with POPOP, the fluorescence of POPOP was completely quenched and the edge emission with narrow spectral peaks became stronger (Fig. 28).

When opal matrices were filled with noncentrally symmetric compounds (Fig. 29), the emission maxima shifted and the emission intensity increased considerably. In this case, the coefficient of conversion of exciting radiation to the secondary emission achieved tens of percent. This suggests that the secondary emission in this case is caused by the three-photon parametric process in which UV photons decompose into two secondary-emission photons, one of which (signal wave) corresponds to a slow photon and another (idler wave) – to IR emission. A similar enhancement of the delayed scattering intensity was observed for opals filled with silver nanoparticles (Fig. 30). In this case, this effect can be explained by a very strong increase in the internal field strength. The effect was observed upon excitation of a globular photonic crystal filled with silver nanoparticles by UV or visible radiation.

Unlike usual three-photon parametric scattering and Raman scattering in common media, the spectrum of spontaneous delayed scattering in a photonic crystal lies in the same region, corresponding to the edges of the forbidden photon band, irrespective of the excitation frequency (if the excitation frequency exceeds the frequency of edge photons).

9. Single-photon-excited delayed scattering of light in globular photonic crystals exposed to repetitively pulsed visible laser radiation

To specify the nature of the secondary emission in opals, we analysed its properties upon excitation of opals by a repetitively pulsed copper vapour laser. We studied initial opals (Fig. 31) and opals filled with centrally symmetric (Fig. 32) and noncentral (Figs 33–35) media.

Secondary emission in opals was excited at a wavelength of 510.6 nm. In this case, the energy of exciting photons lies within the forbidden band (for the normal incidence of light), near its low-energy edge. The pulse repetition rate of the copper vapour laser was 10^4 Hz and the minimal power was 10^4 W. The intensity of the secondary emission of opal matrices filled with nonlinear-optical compounds (ammonium dihydrophosphate, sodium nitrite or MNA) was comparable with that of the excitation line (Figs 33–35).

Of special interest is the results obtained for opal matrices filled with gold or silver particles. In this case,

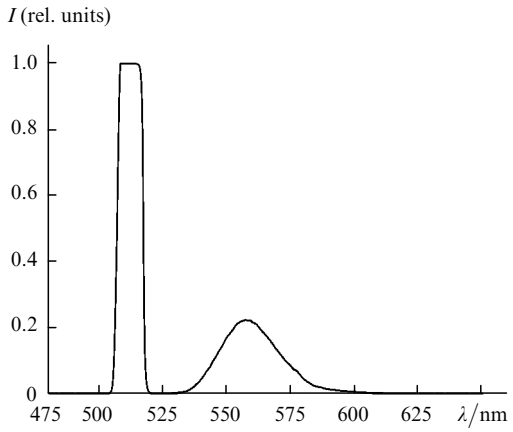

Figure 31. Emission spectrum of initial opal excited by a copper vapour laser at 510.6 nm.

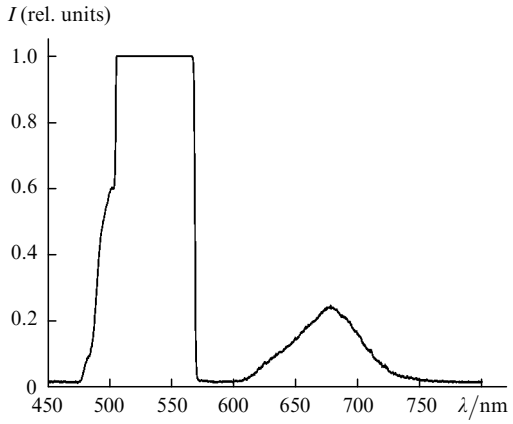

Figure 32. Emission spectrum of opal filled with POPOP excited by a copper vapour laser at 510.6 nm.

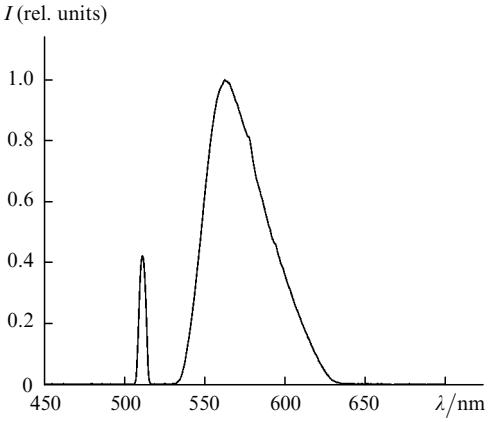

Figure 33. Emission spectrum of opal filled with ammonium dihydrophosphate excited by a copper vapour laser at 510.6 nm.

the secondary emission intensity drastically increases, amounting to tens of percent of that of the excitation line even for opals not filled with noncentral dielectrics. The emission spectrum is located near the low-frequency edge of the forbidden band of opal. The surface-enhanced Raman scattering of light in molecules near gold, silver, platinum, and other metal nanoparticles is well known in modern optics. This effect is explained by a drastic increase

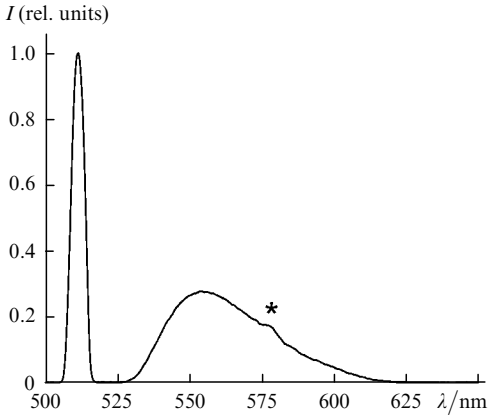

Figure 34. Emission spectrum of opal filled with $NaNO_2$ excited by a copper vapour laser at 510.6 nm. The asterisk indicates a discharge line.

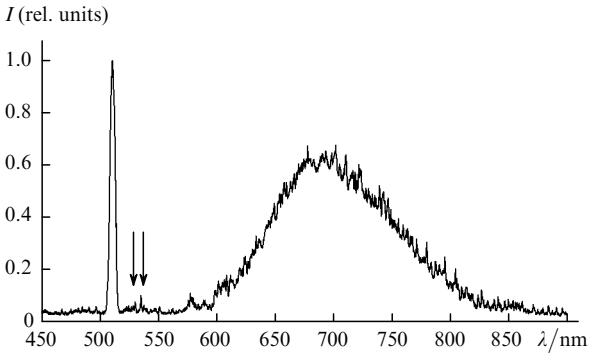

Figure 35. Emission spectrum of opal filled with MNA excited by a copper vapour laser at 510.6 nm. The arrows indicate Raman lines, and the broad band is luminescence of MNA molecules.

in the effective field near metal nanoparticles, which is similar to the increase in this field near a metal edge. The specific feature of this effect in our case is the formation of the ordered bulk structure by metal nanoparticles in the form of a crystal lattice, which opens up new possibilities for the enhancement of the effect. Thus, we found that the intensity of emission of artificial opals in the region close to the stop-band edges excited by a repetitively pulsed laser increases considerably in opals filled with noncentral media for which three-photon parametric scattering proves to be allowed. This confirms the assumption that the secondary emission of opals is related to three-photon parametric scattering of light accompanied by the appearance of slow photons. The secondary-emission intensity can also increase in this case due to Raman scattering because the frequency shift with respect to the exciting line lies within the range of optical vibrations of the corresponding crystal lattices. Because the secondary-emission spectrum lies in the region of the stop-band edge, we can claim that delayed scattering takes place in this case.

Delayed scattering observed in artificial opals in the spectral region of stop-band edges can be used in the future for the development of new light sources. The emission region can be varied in a broad range depending on the size of opal nanoparticles or the filler type.

10. Spontaneous Raman scattering in pure opal matrices and opal matrices doped with dielectrics

Artificial opal matrices are based on amorphous silica a-SiO_2. It is known that the structure of silica glasses, in particular, fused silica is close to that of amorphous silica. The Raman spectra of fused silica excited by an argon laser at 514.5 nm and recorded for different polarisation geometries [19] are presented in Fig. 36. One can see that the Raman spectrum of fused silica exhibits the intense polarised band at 500 cm^{-1} caused by vibrations of the SiO_4 tetrahedrons. The spectrum also contains weak high-frequency bands caused by vibrations of oxygen and silicon. A broad band observed in the low-frequency region at 60 cm^{-1} for both polarisation geometries represents the boson band caused by the formation of quasi-crystalline clusters of size 2–4 nm. On passing from fused silica to a globular photonic crystal, the molecular structure becomes more complicated. One can assume that real amorphous silica globules consist of a few types of clusters whose vibrations should be also manifested in the corresponding frequency region of the inelastic scattering spectrum. In this connection it is interesting to analyse Raman spectra of initial opals.

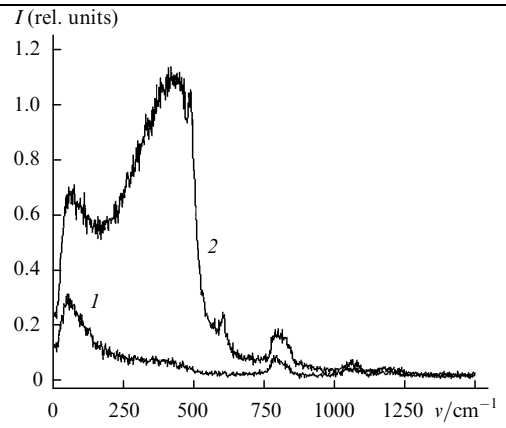

Figure 36. Raman spectra of fused silica corresponding to the Porto geometry $y(xy)z$ (*1*) and $y(xx)z$ (*2*). The polarised band at 60 cm^{-1} is the boson peak.

The analysis of these spectra is complicated due to parasitic scattering caused by microscopic inhomogeneities in real opals and parametric scattering appearing when the excitation wavelength is close to the photon-band edge, as in the case of excitation at 514.5 nm. For this reason it is more convenient to use excitation by laser lines in the red or near-IR spectral regions. Figure 37 presents Raman spectra of an opal matrix and fused silica excited by a 1060-nm Nd : YAG laser [19].

One can see from Fig. 37 that Raman spectra of artificial opal and fused silica are similar. A small difference is observed in the low-frequency region, which can be explained by the presence of additional nanoclusters in artificial opal. A rather intense 1600-cm^{-1} band in the Raman spectrum of opal is probably caused by molecular components contained in opal.

Figures 38 and 39 present Raman spectra of opal filled with a ferroelectric (sodium nitrite) and of polycrystalline sodium nitrite. Good correlation between the spectra of

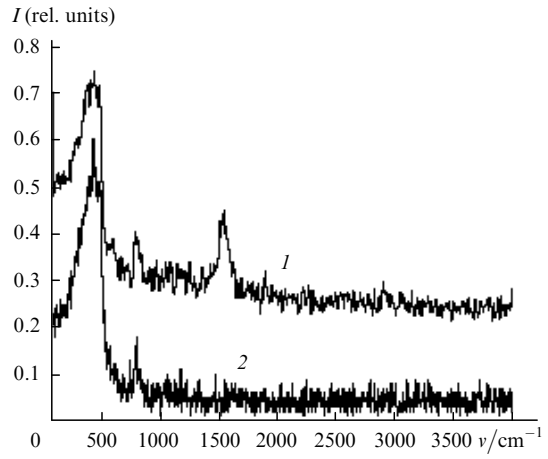

Figure 37. Raman spectra of opal (*1*) and fused silica (*2*).

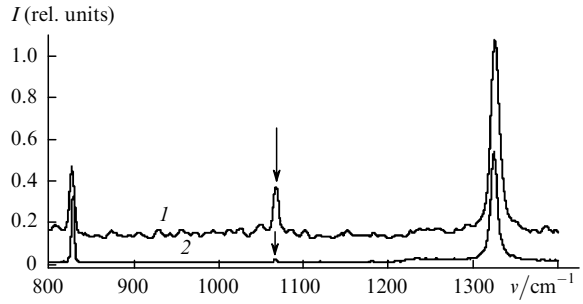

Figure 38. Raman spectra of opal filled with sodium nitrite (*1*) and polycrystalline sodium nitrite (*2*) nanoparticles in the range from 800 to 1400 cm^{-1}. The arrows show Raman lines.

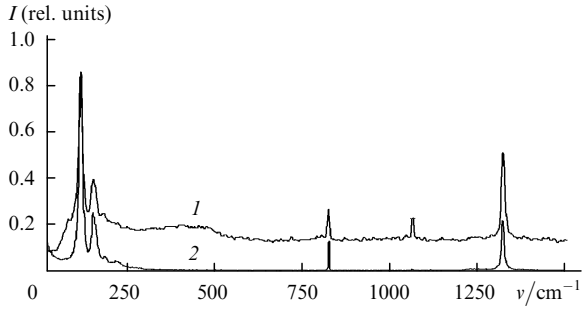

Figure 39. Raman spectra of opal filled with sodium nitrite (*1*) and polycrystalline sodium nitrite (*2*) nanoparticles in the range from 0 to 1500 cm^{-1}.

macro- and microparticles is observed. Note at the same time that the relative intensities in these spectra are redistributed and Raman lines exhibit small shifts.

Figure 40 shows the Raman spectrum of opal filled with sodium nitrite recorded in the $0-4000\text{-cm}^{-1}$ frequency range. The weak bands observed in the high-frequency region cannot be assigned to the fundamental vibrations of the $NaNO_2$ molecule. They are related to the method of composite preparation. Because sodium nitrate introduced into opal matrices was dissolved in ethanol, the high-frequency bands observed in the spectrum belong to ethanol molecules contained in pores, which are probably bound to amorphous silica.

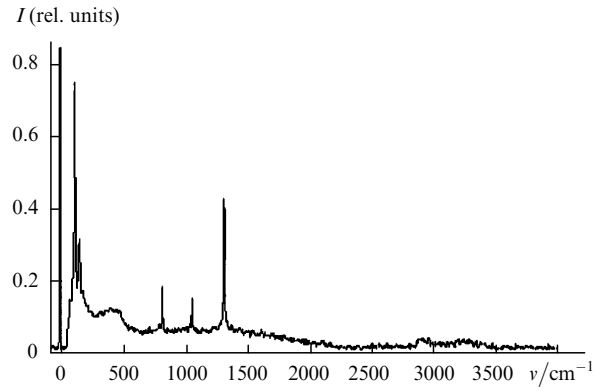

Figure 40. Raman spectra of opal filled with sodium in the range from 0 to 4000 cm^{-1}.

Of special interest is the possibility of observing resonance Raman scattering in molecules embedded into pores of opal matrices and also giant Raman scattering, when silver nanoparticles and a molecular compound to be analysed are doped to pores of opal matrices. Thus, opal matrices filled with dielectrics can be used as supersensitive sensors of molecular structures.

New possibilities are also opened up for optimisation of excitation regimes and lowering the SRS thresholds by filling opal matrices with SRS-active substances such as carbon disulfide, benzene, liquid nitrogen and others.

11. Spontaneous globular scattering of light in opals excited by cw visible laser radiation

In each of the globules of a photonic crystal the standing waves are produced. In the simplest case, the resonator-mode frequency can be found from the expression $\omega = s\pi/d$, where s is the sound speed inside a globule. Resonator modes in globules of a photonic crystal correspond to motions changing the globule size. Excitation can transfer from one globule to another in the photonic crystal, i.e. a globular wave can propagate in the crystal. The corresponding quasi-particles can be called globulons and inelastic light scattering accompanied by excitation of globular waves can be called globular scattering. In the case of low-intensity pumping, such scattering occurs spontaneously. Although the nature of globular scattering is close to that of Raman and Brillouin scattering, unlike the latter, globular scattering can be observed both in the forward and backward directions, and the frequency shift upon globular scattering is considerably smaller than upon Raman scattering, being a few tenths of cm^{-1}.

The spectra of backward global scattering excited by an argon laser at 514.5 nm were recorded for the first time in paper [29]. Synthetic opals with globules of diameters 204, 237, 284, and 340 nm were studied. Figure 41 demonstrates a typical spectrum of spontaneous globular scattering observed in these experiments. The spectrum exhibits six well-resolved lines in the Stokes and anti-Stokes regions at the frequencies of resonator modes in the region from 7 to 27 GHz (1 cm^{-1} corresponds to 3×10^{10} Hz). The presence of the anti-Stokes lines is explained by a high population of low-lying energy levels at room temperature. The position of these lines and their relative intensity are independent of polarisation and the angle of incidence of exciting radiation.

In addition, the parameters of these lines do not change upon the rotation of samples around the normal to their surface at the point of incidence of exciting radiation. Because the diameters of globules in the opal crystal are identical to a high accuracy (3 %), the lines in the scattering spectrum are well-resolved.

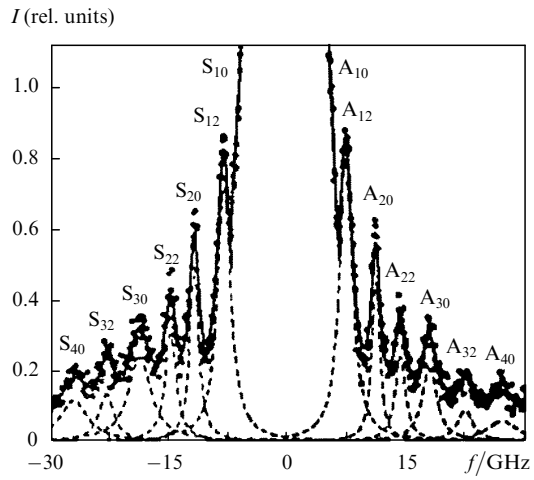

Figure 41. Spontaneous globular scattering spectrum [27].

The experimental results were analysed by using the theory of resonator modes in a homogeneous elastic sphere with a free surface, which was developed by Lamb [30]. Lamb predicted the existence of the two types of globular vibrations characterised by the quantum numbers q and r.

Let us introduce the dimensionless quantities

$$\xi_{rq} = \frac{\pi f_{rq} d}{V_{\text{lon}}}, \qquad \eta_{rq} = \frac{\pi f_{rq} d}{V_{\text{tr}}} \tag{45}$$

characterising these modes. Here, f_{rq} is the acoustic-mode frequency and V_{lon} and V_{tr} are the longitudinal and transverse sound speeds in a globule, respectively.

The equation for the eigenvalues corresponding to acoustic modes excited in the globule during light scattering has the form

$$2\left\{\eta^2 + (l-1)(l+2)\left[\frac{\eta j_{q+1}(\eta)}{j_q(\eta)} - (l+1)\right]\right\}\frac{\xi j_{q+1}(\xi)}{j_q(\xi)} - \frac{1}{2}\eta^4$$

$$+(l-1)(2l+1)\eta^2\left[\eta^2 - 2l(l-1)(l+2)\right]\frac{\eta j_{q+1}(\eta)}{j_q(\eta)} = 0, \tag{46}$$

where η and ξ are the corresponding eigenvalues and $j_q(\eta)$ is the spherical Bessel function of the first kind.

The obtained experimental results were used to determine sound speeds in globules forming the crystal. The values $V_{\text{lon}} = 5279$ m s^{-1} and $V_{\text{tr}} = 3344$ m s^{-1}, which well agree with the known values for fused silica, provide the best agreement with the experimental spectrum.

Because experiments were performed with crystals consisting of globules of different sizes, it was possible to verify experimentally the dependence of the acoustic-mode frequency on the globule diameter. It is known from acoustics that the resonance frequencies in a globule are inversely proportional to its diameter d. The experimental values are well described by the expression

$$f_{rq} = \frac{f_0(r,q)}{d}, \tag{47}$$

where $f_0(r,q)$ is a function depending on the quantum numbers r and q.

Note that elementary excitations appearing during globular excitation of light do not interact with electromagnetic waves, i.e. the corresponding states classified by the even symmetry types are dark states, and quasi-particles produced in elementary scattering processes are darktons.

12. Stimulated globular scattering of light upon pulsed excitation

Opal matrices can be rather easily filled with silica-wetting molecular liquids such as water, ethanol, acetone, benzene, etc. Molecular liquids are typical objects in which different types of stimulated light scattering such as SRS, stimulated Brillouin scattering (SBS), etc. are observed. Until recently, stimulated light scattering in globular photonic crystals was not studied. Stimulated globular scattering (SGS) in opal matrices and artificial opals filled with molecular liquids was first investigated in [18].

Opals were excited by 20-ns, 0.3-J giant pulses from a Q-switched 694.3-nm ruby laser. The divergence of laser radiation was 3.5×10^{-4} rad and the laser linewidth was 0.015 cm^{-1}. Scattering was studied in the forward and backward directions. The corresponding experimental setups are shown schematically in Figs 42 and 43.

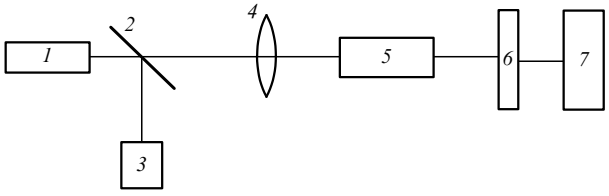

Figure 42. Scheme of the experimental setup for measuring forward SGS: (*1*) ruby laser; (*2*) beamsplitter; (*3*) power meter; (*4*) focusing lens; (*5*) photonic crystal; (*6*) Fabry–Perot interferometer; (*7*) device for recording spectra.

Stimulated globular scattering was excited by focused radiation from a ruby laser. We used in experiments lenses with different focal distances (50, 90, and 150 mm). Positions of samples with respect to a focusing optics also were different. This allowed us to perform measurements at different incident power densities and different field distributions inside samples. We studied scattering in an artificial opal crystal and in opal crystals in which voids between globules were filled with nonlinear liquids (acetone and ethanol). Spectral measurements were performed by using a Fabry–Perot interferometer with two bases providing the free spectral ranges 0.42 and 1.67 cm^{-1}.

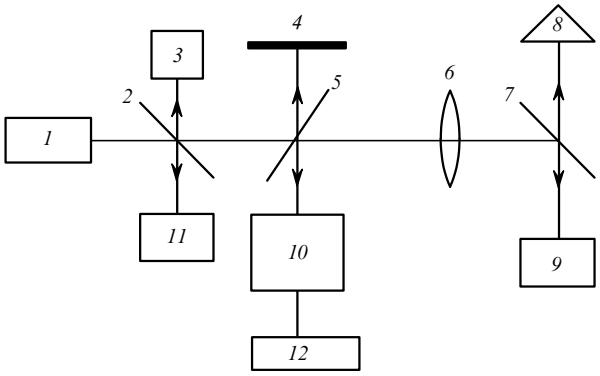

Figure 43. Scheme of the experimental setup for measuring backward SGS: (*1*) ruby laser; (*2*, *5*, *7*) beamsplitter; (*3*, *8*, *11*) power meter; (*4*) removable mirror; (*6*) focusing lens; (*9*) photonic crystal; (*10*) Fabry–Perot interferometer; (*12*) device for recording spectra.

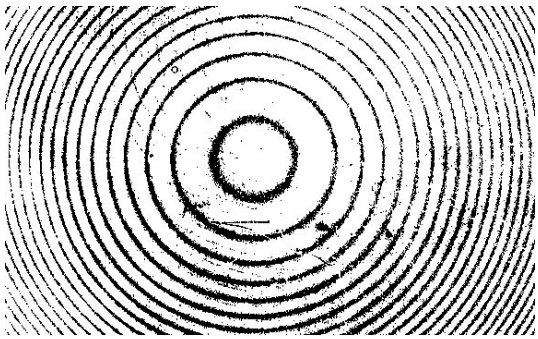

Figure 46. Interferograms of the backward SGS spectrum for an initial (not filled with a molecular liquid) photonic crystal. The free spectral range is 0.833 cm^{-1}. SGS is recorded in the absence of a mirror (see Fig. 43).

We obtained the spectra of exciting radiation and Stokes components caused by vibrations of silica globules in pure opals and opals impregnated with these liquids.

Figure 44 presents the interferogram of the emission spectrum of a ruby laser used in [18]. The width of concentric rings in Fig. 44 gives the laser linewidth 0.015 cm^{-1} in our case.

The backward scattering spectrum of an unfilled opal matrix (Fig. 45) exhibits only one Stokes component shifted with respect to the excitation line by 0.4 cm^{-1} [18]. In this case, double rings are observed which correspond to the ruby laser (larger-diameter ring) and backward SGS (smaller-diameter ring). If mirror (*4*) (Fig. 43) reflecting laser radiation is removed, only single rings corresponding to backward SGS will remain (see Fig. 46). In this case, the SGS linewidth is close to the exciting linewidth and is 0.015 cm^{-1}. This demonstrates a high coherence and high directivity of SGS (strictly backward) and the diffusion scattering of radiation without the frequency shift.

The interference patterns of backward scattering in nanocomposite photonic crystals filled with ethanol exhibited one (for the pump power density 0.12 GW cm^{-2}, Fig. 47a) or two (for the pump power density 0.21 GW cm^{-1}, Fig. 47b) types of the Stokes SGS rings.

Thus, under certain experimental conditions, the two Stokes components corresponding to two types of vibrations of silica globules were observed. This effect took place for opals impregnated with ethanol or acetone. The SGS linewidth for both components was 0.015 cm^{-1}.

Note that after the impregnation of an opal matrix with ethanol or acetone, the sample became virtually transparent.

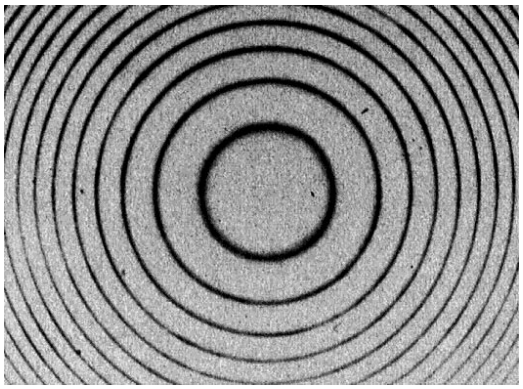

Figure 44. Interferogram of the 694.3-nm emission line of a ruby laser.

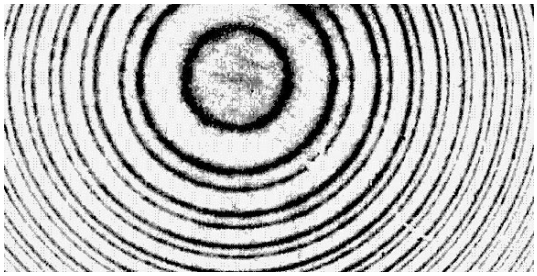

Figure 45. Interferograms of the backward SGS spectrum for an initial (not filled with a molecular liquid) photonic crystal and of the emission spectrum of a 694.3-nm ruby laser. The free spectral range is 0.833 cm^{-1}. Hereafter, larger-diameter rings correspond to laser radiation, and smaller-diameter rings – to SGS.

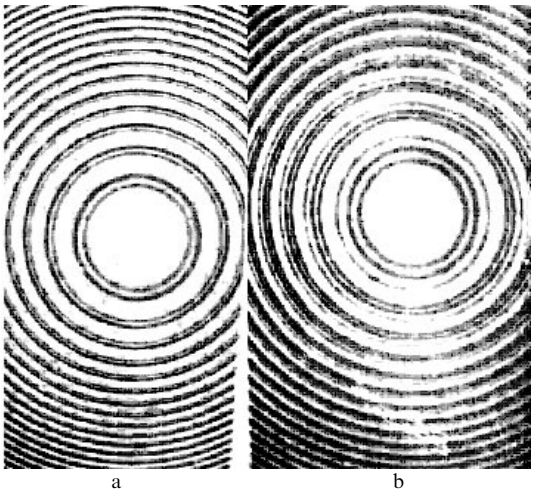

Figure 47. Interferograms of the backward SGS spectrum for a photonic crystal filled with acetone and of the emission spectrum of a 694.3-nm ruby laser for the pump power density 0.12 GW cm^{-2} (a) and 0.21 GW cm^{-2} (b).

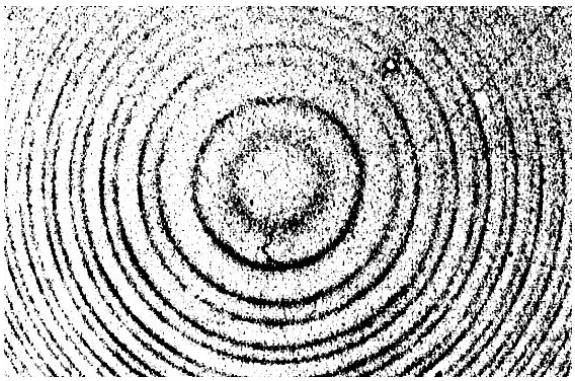

Figure 48. Interferograms of the forward SGS spectrum for a photonic crystal filled with acetone and of the emission spectrum of a 694.3-nm ruby laser. The dispersion region is 1.67 cm^{-1}.

This is explained by the fact that the refractive indices of components of the opal matrix are almost identical.

Our experiments showed that SGS was observed both in the forward and backward directions (Fig. 48), unlike SBS where the forward scattering is absent.

Table 1 presents the frequency shifts of the Stokes components for forward and backward scattering. One can see that the Stokes SGS shifts in opals filled with liquids are close to the SBS shifts in these liquids. Thus, SGS was observed both for unfilled artificial opals and opal nanocomposites in which voids between globules are filled with molecular liquids (acetone or ethanol). We have managed to observe SGS by focusing giant pulses from a ruby laser with a peak power of 10^7 W to opals with a lens with a focal distance of 50 mm. The SGS spectra were recorded in the absence of breakdown in opals.

Table 1. Stokes shifts of the SGS frequencies for forward and backward scattering.

Scattering geometry	Frequency shift/cm^{-1}	Number of Stokes components
Backward SGS in initial opal	0.44	1
Backward SGS in opal filled with acetone	0.40 0.60	2
Forward SGS in opal filled with acetone	0.40	1
Backward SGS in opal filled with ethanol	0.39 0.63	2
Forward SGS in opal filled with ethanol	0.37	1

Excitation of opal matrices filled with dielectrics should induce other nonlinear processes, in particular, SRS, three- and four-photon parametric processes, nonlinearly excited luminescence, generation of optical harmonics, hyper-Rayleigh and hyper-Raman scattering of light.

Not also that both spontaneous and stimulated globular scattering of light gives information on the spectrum of normal vibrations of globules of different types, including spherical nanoparticles in heterogeneous media, protein globules, viruses, etc. In the case of SGS, vibrations of all globules of a photonic crystal prove to be in phase.

13. Opal matrices as active media

Until recently, solid active media for optical pumping were mainly prepared by doping glasses or single crystals with rare-earth ions. New materials include transparent ceramics containing nanopores, which can be filled with an active medium. The size of nanopores and the distance between them change randomly inside a ceramic sample. In this connection globular photonic crystals are of great interest because the size of pores and distance between them are invariable inside an opal matrix. Another important advantage of opals as active media is the possibility of a drastic decrease in the lasing threshold when slowtons are produced during emission. The emission probability increases compared to that in a homogeneous medium due to a drastic increase in the density of photon states near the forbidden-band edge.

Active media of this type based on globular photonic crystals were prepared, for example, in paper [31]. To obtain lasing at 1.54 μm, erbium oxide was doped into pores of an opal matrix. Experiments showed that the quantum yield of luminescence drastically increased with increasing the concentration of Er^{3+} ions, whereas in laser glasses the concentration quenching was observed. One of the methods for filling pores with rare-earth elements is the use of aqueous nitrates of rare-earth ions ($ErNO_3$ and $YbNO_3$).

Of great interest is also the possibility of lasing in the visible region in opal matrices with pores filled with rare-earth ions. From this point of view, dysprosium ions emitting narrow bands in the green spectral region are quite promising (Fig. 49, see [10]).

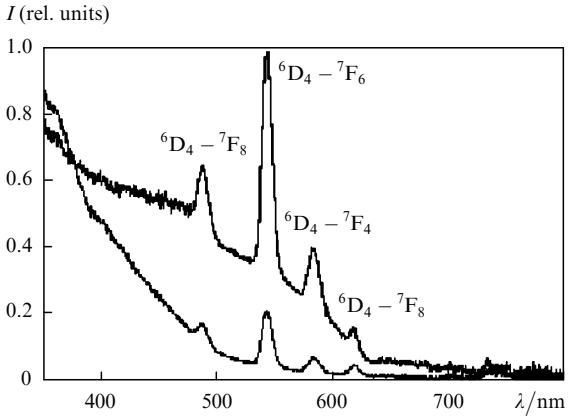

Figure 49. Emission spectrum of opal filled with dysprosium oxide excited by a UV lamp. The two curves correspond to two surfaces of the sample.

The inverse population in semiconductor quantum dots or dye molecules embedded into pores of opal matrices can be achieved upon broadband pumping or pumping by radiation at the frequency close to the low-frequency edge of the stop-band or the absorption band of dye molecules. Lasing can be also obtained in the visible or even UV range by using up-conversion and frequency summation by doping opal pores with nonlinear-optical compounds (sodium nitrite, potassium dihydrophosphate, MNA, and others).

As mentioned in the analysis of secondary emission in opal matrices and nanocomposites, optical excitation of

such systems also leads to parametric emission in a narrow spectral range near the forbidden-band edges. One can expect that this emission will be coherent when proper selective spectral elements, optical resonators and intense pumping are used, which will open up the possibilities for the development of lasers of new types. It is important that lasing in this case is provided not due to the inverse population but due to stimulated emission during stimulated light scattering. Variations in the size of nanoparticles in the opal matrix or in the refractive indices of components of the matrix provide tuning of the laser wavelength in a broad spectral range.

14. Resonance and two-photon-excited delayed light scattering in globular photonic crystals

When the excitation frequency is detuned far enough from the edges of the forbidden photon band, three-photon parametric processes make the main contribution to excitation of the slowton states, as mentioned above. In this case, due to the anomalous increase in the density of photon states near the band edges, the threshold of transition from spontaneous parametric scattering to lasing is lower than the corresponding threshold in homogeneous nonlinear media.

In the case of small detuning of the excitation frequency, Raman processes, which are enhanced due to a drastic increase in the density of photon states near the forbidden-band edges, can also make a considerable contribution to the creation of slowtons. If the excitation frequency coincides with one of the frequencies corresponding to the low- or high-frequency edge of the forbidden band, the resonance excitation of slowtons should take place. The corresponding light scattering can be called resonance delayed scattering.

Figures 50 – 52 present the secondary emission spectra of opals observed when the excitation frequency approaches the forbidden-band edge. The secondary emission was excited by semiconductor diodes at 381.5, 463.0, and 530.0 nm. One can see from Fig. 50 that the secondary emission spectrum of opal filled with POPOP changes its shape when the excitation wavelength approaches the stop-band edge: the intensity of the secondary emission band increases and the position of the intensity maximum approaches the excitation band. The spectrum in Fig. 50c corresponds to resonance delayed scattering. The spectrum consists of one band, which has a shape close to that of the excitation band, but is shifted to the Stokes region. Similar situations take place for initial opal (Fig. 51) and opal filled with sodium nitrite (Fig. 52). In this case, the resonance is achieved both for the lower and upper edges of the stop-

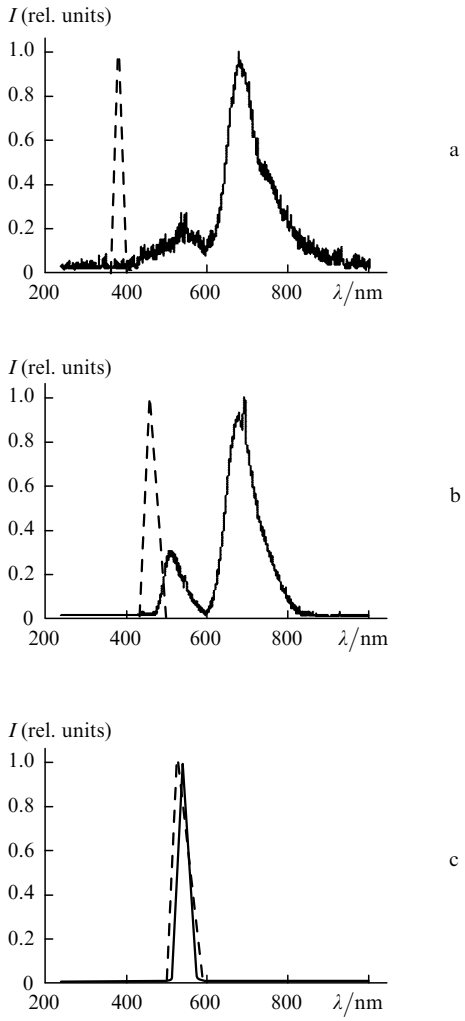

Figure 50. Emission spectra of opal filled with POPOP excited by semiconductor LEDs at 381.5 (a), 463.0 (b), and 530 nm (c). The dashed curves are excitation lines.

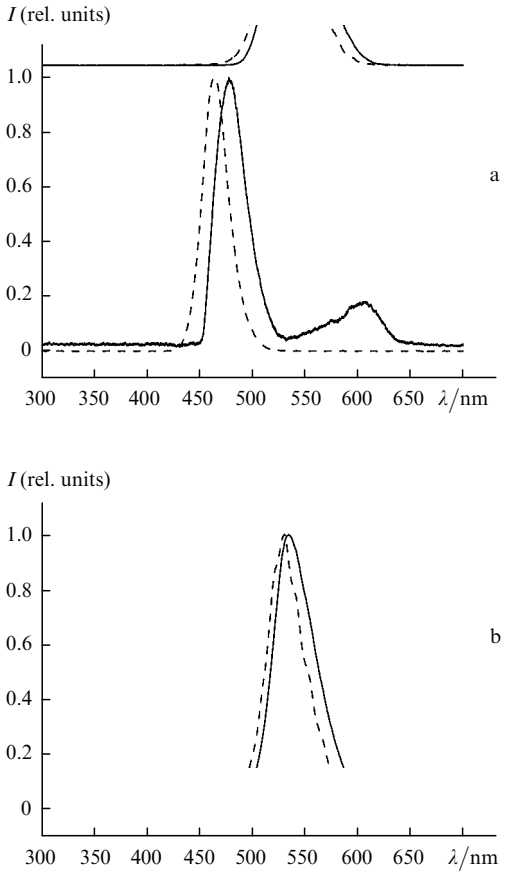

Figure 51. Spectra of the resonance delayed scattering for initial opal excited by semiconductor LEDs at 463.0 (a), and 530 nm (b). The dashed curves are excitation lines.

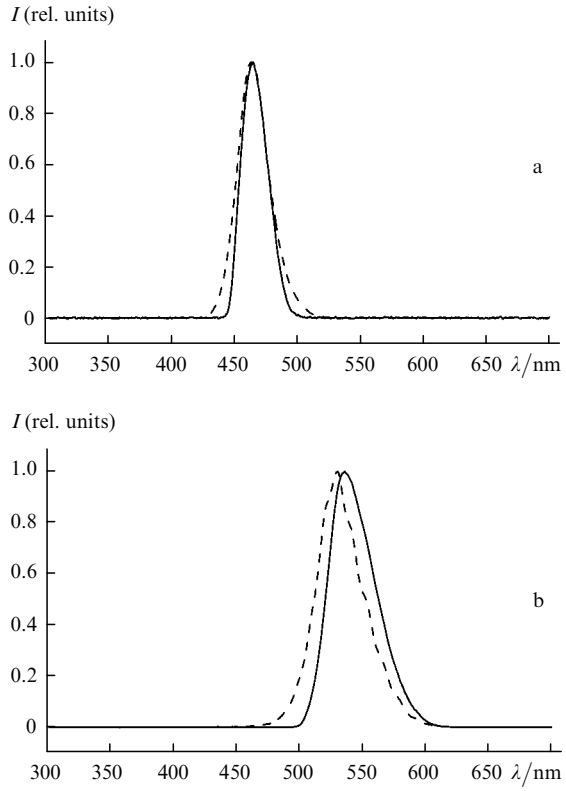

Figure 52. Spectra of the resonance delayed scattering for opal filled with sodium nitrite excited by semiconductor LEDs at 463.0 (a), and 530 nm (b). The dashed curves are excitation lines.

band. The frequencies corresponding to the slowton states can be estimated from the measured frequencies of the maxima of resonance delayed scattering.

The elementary process of four-photon parametric scattering of light involves the simultaneous annihilation of two exciting photons accompanied by the creation of two secondary-emission photons. According to the properties of the perturbation operator, this process is allowed by the selection rules both for noncentrally symmetric and centrally symmetric media. The laws of conservation of energy and quasi-momentum in the elementary process of four-photon parametric scattering in a globular photonic crystal have the form ($\hbar = 1$)

$$2\omega_0 = \omega_1 + \omega_2, \qquad 2\boldsymbol{k}_0 = \boldsymbol{k}_1 + \boldsymbol{k}_2 + \boldsymbol{b}_i. \tag{48}$$

Here, ω_0 is the frequency of the exciting photon and ω_1 and ω_2 are frequencies of the two created photons. Because this process is nonlinear, quite intense excitation is required to observe it. The threshold of transition from spontaneous emission to lasing is considerably reduced if one of the created photons (for example, with frequency ω_1) is a slowton. Consider the results of experimental study [32] performed recently in this field. Photonic crystals were excited by 20-ns, 0.3-J giant pulses from a 694.3-nm ruby laser (Fig. 53). The divergence of laser radiation and the laser linewidth were 3.5×10^{-4} rad and $0.015\ \mathrm{cm}^{-1}$, respectively. Forward and backward scattering excited by a focused laser beam (in the absence of a spark) was

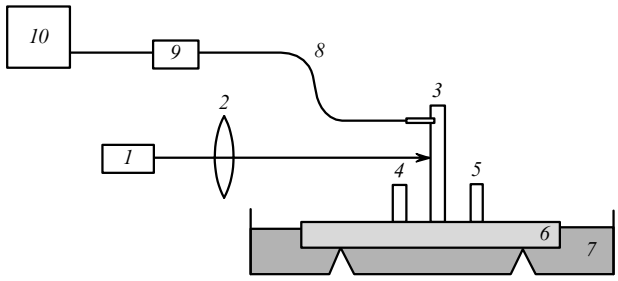

Figure 53. Scheme of the experimental setup for excitation of opals by giant pulses from a ruby laser; (*1*) ruby laser; (*2*) focusing lens; (*3*, *4*, *5*) crystals under study; (6) cold finger; (*7*) cell with liquid nitrogen; (*8*) optical fibre; (*9*) spectrometer; (*10*) computer.

studied. The radiation power density inside samples was $10-100\ \mathrm{MW\ cm}^{-2}$. Samples were thin oriented plates of globular photonic crystals with the (111) surface, which were mounted on a cold finger cooled to 78 K.

Globular photonic crystals excited by giant pulses from a ruby laser emitted anti-Stokes (blue–green) radiation of intensity comparable with the pump intensity during the laser pulse. The emission was analysed with a digital camera in the specified-exposure regime or by using a frame sweep with an interval of 0.01 s. The emission spectra were analysed by using a FSD8 mini spectrometer. Figure 54 presents the photographs of emission observed during the laser pulse and approximately 1 s after the pulse end. Along with the red emission of the ruby laser, the blue–green emission is observed in the focal region of exciting radiation. The secondary blue–green emission was observed in opal for 3–5 s after the end of the 20-ns laser pulse. Another important feature of this emission is that it was observed not only in a sample in which the exciting radiation was focused but also in samples located at a distance of ~ 1 cm from the excited sample (Fig. 55). A long duration of the secondary emission confirms the excitation of slowtons in the blue–green spectral range (see Fig. 50).

This effect was most distinctly observed at low temperatures (close to liquid nitrogen temperature). The intensity of blue–green emission drastically changed depending on the sample orientation, i.e. the fulfilment of the synchronism condition was required to observe the emission. The effect had a threshold and appeared at the power density of $10^7\ \mathrm{W\ cm}^{-2}$, which demonstrates the stimulated nature of this emission. Note that the emission intensity changed nonmonotonically, i.e. intensity oscillations were observed. In some cases, the blue–green emission virtually disappeared at a certain instant after the end of the pump pulse and then appears again.

This effect can be interpreted as the observation of two-photon-excited delayed light scattering in a globular photonic crystal. Delayed light scattering can be treated as a new type of stimulated scattering of light because it has a threshold. Such scattering leads to the generation of slowtons in the blue–green spectral region in a globular photonic crystal upon two-photon pumping. In this case, at the first stage of the elementary scattering process the two exciting photons are absorbed, while at the second stage a slowton is created in the blue–green spectral region corresponding to the Brillouin-zone edge, and a complementary photon in the IR region. A long duration of the

Figure 54. Photographs of emission of the opal surface during the laser pulse (a) and ~1 s after the end of the pulse (b).

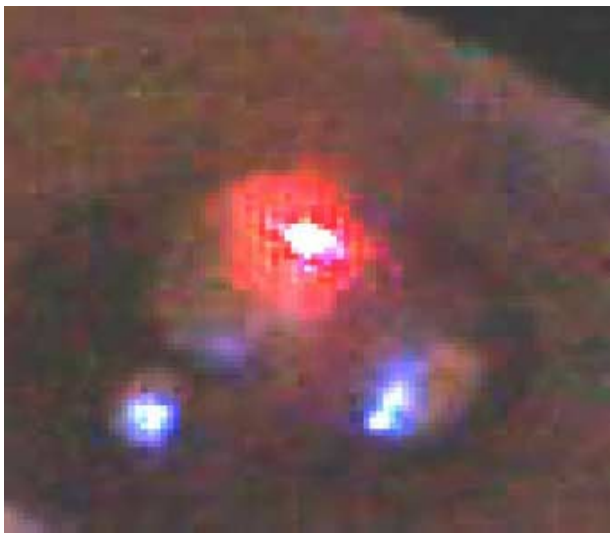

Figure 55. Photograph of emission of crystals located on a copper substrate at liquid nitrogen temperature. The red colour of the upper crystal corresponds to emission of a ruby laser, the blue–green colour of the two lower crystals corresponds to delayed emission of the sample and samples located at a distance of ~1 cm from the irradiated crystal.

blue–green emission is caused by a small propagation velocity of the corresponding electromagnetic waves. Taking into account that the thickness of a photonic crystal plate was 0.1 cm and the emission lifetime was ~1 s, we can assume that the velocity of the corresponding electromagnetic waves inside the sample did not exceed 0.1 cm s^{-1}. The anomalous slowing down of the electromagnetic waves of secondary emission (slowton waves) generated upon two-photon pumping by giant laser pulses provides drastic local increase (by several orders of magnitude) in the radiation energy density inside a photonic crystal. In the case of repetitively pulsed laser excitation, the energy should be accumulated inside the crystal. Thus, the generation of slowton waves in two-photon-excited delayed scattering seems promising for the local heating of a material medium, which can be used to initiate chemical reactions, structural transformations, nuclear reactions, etc.

The intensity oscillations of the long-lived emission can be explained by the creation and subsequent annihilation of biphotons. In this case, the emission intensity decreases when a part of slowtons transforms to biphotons. The annihilation of biphotons leads to an increase in the number of slowtons, resulting in the increase in the secondary-emission intensity.

A special situation appears when the second-harmonic frequency of exciting radiation falls in the forbidden photon band. If the pores of a crystal are filled with noncentral molecules, having a high nonlinearity, the second-harmonic intensity drastically increases. This effect was observed in experiments performed by the author together with N.F. Bunkin and V.D. Shigorin (General Physics Institute, RAS).

Figure 56 demonstrates the efficient conversion of the IR-radiation of a 1064-nm Nd : YAG laser to the green 532-nm radiation in an MNA-doped globular photonic crystal. Thus, globular photonic crystals filled with noncentral molecules with a high nonlinearity can be used as efficient laser frequency converters.

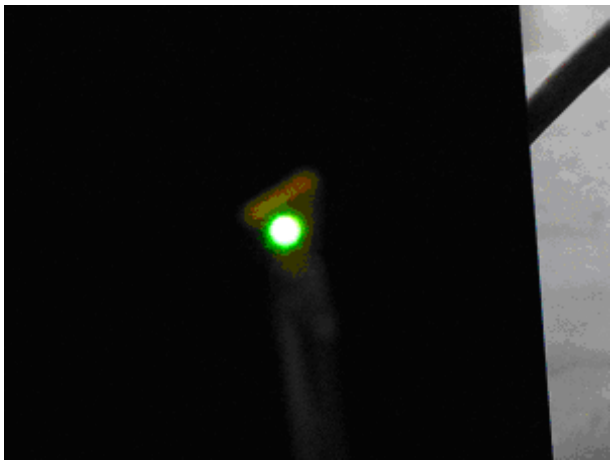

Figure 56. Demonstration of frequency doubling in a globular photonic crystal filled with MNA. The photograph of the 532-nm second-harmonic emission excited by a Nd : YAG laser.

15. Conclusions

Globular photonic crystals have unique optical and nonlinear-optical properties, which open up new opportunities in quantum electronics. It is possible to create new nonlinear-optical elements such as frequency converters, parametric frequency converters, and new types of lasers. The long-lived emission of opal matrices excited by UV or visible radiation can be used for the development of new radiation sources emitting in different spectral regions.

Opal matrices filled with dye molecules or semiconductor quantum dots represent a new type of highly efficient laser media.

Opal matrices filled with nanoparticles of noble metals (silver, gold, platinum) can be used for the giant enhancement of the secondary-emission-excitation efficiency, including Raman scattering, generation of optical harmonics, parametric processes, etc. The stimulated long-lived emission in opals allows one to accumulate the energy of electromagnetic radiation inside a small region of a sample for a few seconds. It is interesting to study in the future the known nonlinear phenomena such as SRS, hyper-Rayleigh and hyper-Raman light scattering, two-photon-excited fluorescence, generation of optical harmonics, etc.

Acknowledgements. The author thank M.I. Samoilovich and S.N. Ivicheva for placing samples at our disposal and their preparation for experiments. This work was supported by the Russian Foundation for Basic Research (Grant Nos 07-02-00106a, 05-02-16205, 06-02-81024-Bela.

References

1. Bykov V.P. Zh. *Eksp. Teor. Fiz.*, **62**, 505 (1972).
2. Yablonovitch E. *Phys. Rev. Lett.*, **58**, 2059 (1987).
3. John S. *Phys. Rev. Lett.*, **58**, 2486 (1987).
4. Astratov V.N., Bogomolov V.N., Kaplyanskii A.A., Prokofiev A.V., Samoilovich L.A., Samoilovich S.M., Vlasov Yu.A. *Nuovo Cimento*, **D 17**, 1349 (1995).
5. Yablonovitch E., Gmitter T.J., Leung K.M. *Phys. Rev. Lett.*, **67**, 2295 (1991).
6. Fogel I.S., Bendickson J.M., Tocci M.D., Bloemer M.J., Scalora C.M., Bowden J.P. *Pure Appl. Opt.*, **7**, 393 (1998).
7. Gorelik V.S., Zlobina L.I., Murzina T.V., Sverbil' P.P., Sychev F.Yu. *Kratk. Soobshch. Fiz. FIAN*, (6), 3 (2004).
8. Gorelik V.S., Zlobina L.I., Sverbil' P.P., Fadyushin A.B., Chervyakov A.V. *J. Russ. Laser Research*, **26** (3), 211 (2005).
9. Gorelik V.S., Burkov V.I., Melnik N.N., Sverbil P.P., Ivicheva S.N., Zlobina L.I., Chervyakov A.V. *Chinese J. Light Scattering*, **17** (3), 268 (2005).
10. Artamonov A.N., Burkov V.I., Vitukhnovskii A.G., Gorelik V.S., Ivicheva S.N., Sverbil' P.P., Skorikov V.M. *Kratk. Soobshch. Fiz. FIAN*, (10), 20 (2005).
11. Artamonov A.N., Burkov V.I., Vitukhnovskii A.G., Gorelik V.S., Ivicheva S.N. *Tez. dokl. III Vseros. konf. 'Neobratimye protsessy v prirode i tekhnike'* (Proc. III All-Union Conf. on Irreversible Processes in Nature and Technique) (Moscow: N.E. Bauman Moscow State Technical University, 2005) p. 278.
12. Gorelik V.S., Zlobina L.I., Sverbil' P.P., Fadyushin A.B., Chervyakov A.V. Preprint FIAN, No. 2 (Moscow: 2005).
13. Gorelik V.S., Zlobina L.I., Manushkin A.A., Samoilovich M.I., Sverbil' P.P., Somenkov V.A., Yurasov N.I. *Trudy XI Mezhdunarod. nauchno-tekhn. konf. 'Vysokie tekhnologii v promyshlennosti Rossii'* (Proc. XI International Scientific and Technical Conf. on High Technologies in the Industry of Russia) (Moscow: Tekhnomash TsNITI, 2005) p. 91.
14. Golub' Yu.Ya., Gorelik V.S., Zlobina L.I., Moiseenko V.N., Sverbil' P.P., in *'Neobratimye protsessy v prirode i tekhnike'* (Irreversible Processes in Nature and Technique) (Moscow: FIAN, 2005) p. 308.
15. Gorelik V.S., in *'Neobratimye protsessy v prirode i tekhnike'* (Irreversible Processes in Nature and Technique) (Moscow: FIAN, 2005) p. 283.
16. Gorelik V.S. *Proc. Int. Scient. Meet. «Physical Interpretations of Relativity Theory»* (Moscow: Coda, 2005) p. 70.
17. Golub' Yu.Ya., Gorelik V.S. *Proc. Int. Scient. Meet. «Physical Interpretations of Relativity Theory»* (Moscow: Coda, 2005) p. 288.
18. Gorelik V.S., Kudryavtseva A.D., Chernega N.V. Preprint FIAN, No. 31 (Moscow, 2005).
19. Avakyants L.P., Gorelik V.S., Zlobina L.I., Mel'nik N.N., Sverbil' P.P., Fadyushin A.B., Chervyakov A.V. *Neorg. Mater.,* **42** (6), 703 (2006).
20. Gorelik V.S. *J. Rus. Laser Research*, **27**, 400 (2006).
21. Gorelik V.S., Esakov A.A., Zlobina L.I., Sverbil' P.P., Samoilovich M.I., Yurasov N.I. *Trudy XI Mezhdunarod. nauchno-tekhn. konf. 'Vysokie tekhnologii v promyshlennosti Rossii'* (Proc. XI International Scientific and Technical Conf. on High Technologies in the Industry of Russia) (Moscow: Tekhnomash TsNITI, 2005) p. 467.
22. Gorelik V.S., Esakov A.A., Fadyushin A.B. Preprint FIAN, No. 14 (Moscow, 2006).
23. Vlasov Yu.A., Astratov V.N., Baryshev A.V., Kaplyanskii A.A., Karimov O.Z., Limonov M.F. *Phys. Rev. E*, **61**, 5784 (2000).
24. Golubev V.G., Kosobukin V.A., Kurdyukov D.A., Medvedev A.V., Pevtsov A.B. *Fiz. Tekh. Poluprovodn.*, **35**, 710 (2001).
25. Balakirev V.G., Bogomolov V.N., Zhuravlev V.V., Kumzerov Yu.A., Petranovskii V.P., Romanov S.G., Samoilovich L.A. *Kristallografia*, **38**, 111 (1993).
26. Baryshev A.V., Kaplyanskii A.A., Kosobukin V.A., Limonov M.F., Samusev K.B., Usvyat D.E. *Fiz. Tverd. Tela*, **45**, 434 (2003).
27. Yari A., Yeh P. *Optical Waves in Crystals* (New York: Wiley, 1987).
28. Sakoda K. *Optical Properties of Photonic Crystals* (Berlin: Springer, 2001).
29. Kuok M.H., Lim H.S., Ng S.C., Liu N.N., Wang Z.K. *Phys. Rev. Lett.*, **90**, 255502 (2003).
30. Lamb H. *Proc. London Math. Soc.*, **13**, 189 (1882).

31. Samoilovich M.I., Belyanin A.F., Kleshcheva S.M., Tsvetkov M.Yu., Zhitkovskii V.D., Gur'yanov A.V. *Trudy XI Mezhdunarod. nauchno-tekhn. konf. 'Vysokie tekhnologii v promyshlennosti Rossii'* (Proc. XI International Scientific and Technical Conf. on High Technologies in the Industry of Russia) (Moscow: Tekhnomash TsNITI, 2005) p. 274.
32. Tcherniega N.V., Kudryavtseva A.D. *J. Rus. Laser Research*, **27** (5), 450 (2006).